

**PARAMETERIZATION OF THE SIZE AND SHAPE OF INTRACRANIAL  
SACULAR ANEURYSMS USING LEGENDRE POLYNOMIALS**

A Thesis

by

CORY WAYNE FARLEY

Submitted to the Office of Graduate Studies of  
Texas A&M University  
in partial fulfillment of the requirements for the degree of

MASTER OF SCIENCE

December 2004

Major Subject: Biomedical Engineering

**PARAMETERIZATION OF THE SIZE AND SHAPE OF INTRACRANIAL  
SACULAR ANEURYSMS USING LEGENDRE POLYNOMIALS**

A Thesis

by

CORY WAYNE FARLEY

Submitted to Texas A&M University  
in partial fulfillment of the requirements  
for the degree of

MASTER OF SCIENCE

Approved to style and content by:

---

Jay D. Humphrey  
(Chair of Committee)

---

William A. Hyman  
(Head of Department)

---

Hsin-I Wu  
(Member)

---

Harry A. Hogan  
(Member)

December 2004

Major Subject: Biomedical Engineering

**ABSTRACT**

Parameterization of the Size and Shape of Intracranial Saccular Aneurysms Using

Legendre Polynomials. (December 2004)

Cory Wayne Farley, B.S., Texas A&M University

Chair of Advisory Committee: Jay D. Humphrey

Currently, size is used as the predetermining factor to judge whether a saccular aneurysm is likely to rupture. Recent studies of the nonlinear mechanics of saccular aneurysms suggest that it is unlikely that they enlarge or rupture via material (limit point) or dynamic (resonance) instabilities. Rather, there is a growing body of evidence from both vascular biology and finite element analyses that implicate mechanosensitive growth and remodeling processes. There is, therefore, an even greater need to quantify regional multiaxial wall stresses, which because of the membrane-like behavior of aneurysms implicates the need for better data on regional surface curvatures. By using a convenient function, such as a Legendre polynomial, a quick, accurate approximation can be made for the size and shape of a saccular aneurysm that allows for stress analysis that surgeons can use to determine if the risk of rupture warrants the risk of treatment.

**TABLE OF CONTENTS**

	Page
ABSTRACT .....	iii
TABLE OF CONTENTS .....	iv
LIST OF FIGURES .....	v
LIST OF TABLES .....	vi
INTRODUCTION .....	1
Overview of Research Project .....	2
LITERATURE REVIEW .....	4
PRIOR WORK .....	8
LEGENDRE POLYNOMIALS .....	11
Legendre Functions .....	11
METHODS .....	16
RESULTS .....	20
DISCUSSION .....	25
CONCLUSIONS .....	28
REFERENCES .....	29
APPENDIX 1 .....	33
APPENDIX 2 .....	38
APPENDIX 3 .....	53
VITA .....	58

## LIST OF FIGURES

FIGURE	Page
1      Sample of the MRA images used by Banatwala (2001) .....	8
2      Final surface of a human intracranial saccular aneurysm .....	9
3      Curvature ( $\kappa_1$ ) values for Aneurysm #3 color-coded by range .....	10
4      Variability capable by our chosen function by altering values of $n$ and $m$ .....	12
5      Effects of varying $c$ while keeping other parameters constant .....	13
6      For Aneurysm 3, the values of the maximum curvature values .....	22
7      For Aneurysm 3, the values of the minimum curvature values .....	22
8      Aneurysm 3 Kappa 1 .....	23
9      Aneurysm 3 Kappa 2 .....	24

**LIST OF TABLES**

FIGURE		Page
1	Tabulated results from the various modeling methods .....	21
2	Computation times for modified and unmodified Legendre spheroids .....	24

## INTRODUCTION

An aneurysm is a “sac formed by the dilatation of the wall of an artery” (Dorland Medical Dictionary). More specifically, an intracranial saccular aneurysm (ISA) is an “eccentric localized distended sac affecting only a part of the circumference of the artery wall” (Dorland Medical Dictionary). That is, an ISA is a balloon-like dilatation protruding from the side of an artery. A small percentage (2-5%) of the population harbors an ISA, and only 0.1% of those aneurysms rupture annually. The effects from a rupture, however, are devastating with a mortality rate of 50 to 60% (Orz et al., 1997). Conversely, treatments for saccular aneurysms have a morbidity or mortality rate as high as 17.5% after 30 days (Wiebers, 1998). There exists, therefore, a need to find ways to determine the risk of rupture of an aneurysm quickly and correctly in order to treat all dangerous lesions while not putting too many patients at risk.

Size is the primary parameter currently used to determine whether an aneurysm is likely to rupture or not. Studies show that for large aneurysms (>10mm), treatment is required and the risk of rupture is quite high. For smaller aneurysms (<4mm), however, size alone would suggest that all of these lesions are safe and unlikely to rupture. In reality, some of these small lesions do rupture while larger aneurysms remain stable, which implies a new predictor is needed. The geometry of saccular aneurysms has had little study with only the most basic parameters, such as head-to-neck ratio, being explored as predictors for the rupture of a lesion (Parlea et al., 1999). A few groups have implied that size is not the predetermining driver to rupture, but instead suggest the

surface of the aneurysm to have properties following membrane mechanics, which leads to curvature being the defining factor driving aneurysms to rupture (Elger et al., 1996; Sacks et al., 1999; Vorp et al., 1998). Therefore, there is a need to calculate the curvatures of a lesion quickly and accurately.

Imaging technology has advanced to the point that a 3-D picture of an aneurysm is available, but specific analyses are not. The 3-D coordinates representing the surface can be used to calculate the curvatures and stresses in the membrane of the lesion via a discrete or an analytical method. A true finite element analysis would require an undeformed configuration, which would be very difficult to obtain in vivo. Unloading the aneurysm would mean stopping flow in the artery, and the metabolic needs of the brain would not be met, resulting in stroke or death. Other methods to describe the stresses in the membrane would require knowledge of the properties of the material. Constitutive models for saccular aneurysms have progressed recently thanks to the work of researchers such as Canham et al. (1999) and Mimata et al. (1997); however, such studies are far from being complete enough to be able to accurately estimate the stresses in the wall of the aneurysm. To bypass the aforementioned complications, we use a membrane model for the wall, which seems to hold for idealized axisymmetric aneurysms (Elger et al., 1996; Humphrey, 1998).

### *Overview of Research Project*

The goal of this research is to explore a possible way to modify Legendre spheroids so as to better approximate the size and shape of ISAs. Towards this end, this

this thesis first provides a catalog of Legendre spheroids that are representative of possible lesions and their respective curvatures. Second, for purposes of illustration, best-fit Legendre spheroids are determined for five human lesions, and the principal curvatures are computed and compared to prior results by Banatwala (2001). These prior results are based on both “unmodified” Legendre spheroids and spline fits. In particular, the curvatures are displayed by mapping color-coded values to the surface in a three-dimensional space. In the future, the curvatures can be used in the context of membrane theory to calculate regional stresses.

Finally, this thesis also contains a concise program that allows one to enter a data file containing three-dimensional Cartesian data points that describe the surface of a lesion, and returns a modified Legendre spheroid. This code minimizes error via a Marquardt-Levenberg regression.

## LITERATURE REVIEW

Recall that if an aneurysm ruptures, there is a 50 percent mortality rate, while a 17 percent mortality and morbidity rate results from surgical treatment. Due to the risk involved with treatment, physicians do not want to merely treat every aneurysm they find; however, they must operate on every lesion that has a plausible chance of rupturing. Physicians, therefore, rely on diagnostic techniques to determine if a patient requires surgical treatment for an aneurysm.

Currently, the decision on whether or not to perform surgery is based primarily on the maximum diameter of the aneurysm even though the 'critical diameter' for rupture is disputed. While there is general agreement that aneurysms with a maximum dimension >10mm should be treated surgically, there is disagreement about aneurysms having a maximum dimension <10mm. Zacks et al. (1980) concluded that unruptured aneurysms having a maximum diameter <10mm had a very low probability of rupture, as did Wiebers (1998). This conclusion is in stark contrast to Crompton (1966), who suggested a critical diameter as small as 4mm. Orz et al. (1997) suggested further that the critical diameter varied depending on the location of the aneurysm and concluded that lesions located on the anterior communicating artery are most likely to rupture; they recommended surgery for all of these lesions, regardless of size. In contrast, based on a retrospective study, Hademenos et al. (1998) concluded that lesions of the posterior intracranial circulation are more prone to rupture.

The use of size as the best indicator of rupture-potential is due to the fact that it is the easiest property of an aneurysm to measure. The law of Laplace relates the in-plane

Cauchy stress  $\sigma$  to the distension pressure  $P$ , current radius  $a$ , and current thickness  $h$  for an inflated, thin-walled, spherical structure,

$$\sigma = \frac{Pa}{2h}. \quad (1)$$

Typically, the systolic blood pressure of a patient with an aneurysm would be on the order of 120 to 150 mmHg. Although these values are not tremendously different, they result in a 25% difference in the computed stress. Wall thickness is less well known, but could easily range from 20 to over 200  $\mu\text{m}$ , in turn affecting the computed values of stress by an order of magnitude. Given that the maximum dimension of a saccular aneurysm can range from 1 to 20 mm, this too could affect the computed stress by an order of magnitude. Due to the inability of measuring wall thickness clinically, and the much more modest effect of pressure on the stress, most attention has focused on correlating rupture-potential with the diameter of the lesion. This emphasis is based, however, on a misinterpretation of the law of Laplace. Equation 1 is better interpreted as

$$\sigma = \frac{P}{2h\kappa}, \quad (2)$$

where  $\kappa$  is the curvature; that is,  $a$  from equation 1 is actually the radius of curvature, not the radius. Only in special geometries (e.g. sphere, cylinder) does  $1/\kappa \equiv \text{radius}$ , thus associating the stresses with a value for the maximum diameter applies for special geometries. As applied clinically, therefore, the law of Laplace assumes a spherical geometry, which approximates aneurysmal geometry only in a small sub-class of lesions. In addition, the law of Laplace predicts uniform stress fields, which does not explain the propensity of aneurysms to rupture at the fundus. Based on more realistic geometries,

Humphrey and Kyriacou (1996) and Shah et al. (1997) demonstrated the importance of curvatures in determining stress in particular sub-classes of saccular lesions.

In the case of axisymmetry, for example, the principal stress resultants,  $T_1$  and  $T_2$  can be computed in terms of the maximum and minimum curvatures,  $\kappa_1$  and  $\kappa_2$ , respectively,

$$T_1 = \frac{P}{2\kappa_2} \text{ and } T_2 = \frac{P}{\kappa_2} \left( 1 - \frac{\kappa_1}{2\kappa_2} \right), \quad (3)$$

which not only reveals the importance of the curvatures, but also shows that in special cases, stress resultants can indeed be computed independent of the properties of the material and knowledge of the undeformed configuration (i.e., the principal curvatures  $\kappa_1$  and  $\kappa_2$  are defined in the current configuration). The equations for the principal stress resultants for an ellipsoidal geometry, for example, are given by:

$$T_1 = \frac{Pa^2}{2(a^2 \sin^2 \phi + b^2 \cos^2 \phi)^{1/2}}, \quad (4)$$

and

$$T_2 = \left[ \frac{Pa^2}{(a^2 \sin^2 \phi + b^2 \cos^2 \phi)^{1/2}} \right] \left( 1 - \frac{a^2 \sin^2 \phi + b^2 \cos^2 \phi}{2b^2} \right), \quad (5)$$

where  $a$  and  $b$  are the deformed major and minor dimensions, respectively, and  $\phi \in [0, \pi]$  is the angle between the axis of symmetry and the line connecting the origin and the point of interest (Humphrey, 1998). The result for a sphere is recovered when  $a = b$ . Thus, stress resultants can be calculated easily when one can model the lesion by a spherical or ellipsoidal geometry.

Although spherical and ellipsoidal geometries can approximate well certain subclasses of lesions, many other lesions are clearly more complex in shape. There is a need, therefore, to account for such complexities. In this thesis, Legendre functions of the first kind are introduced to provide improved descriptions of aneurysmal geometry while still providing an equation that can be analyzed easily. These functions have the added benefit that very different shapes can be described via a few parameters. Even in the absence of in vivo data, these equations can be used to create idealized sub-classes of aneurysms for the purpose of analysis.

Based on this literature search, very little work has been done on the calculations of curvature from clinical data on aneurysms. The exception is the work done by Sacks et al. (1999) on abdominal aortic aneurysms, which presented a method for calculation of curvatures from magnetic resonance angiography (MRA) data. Marrisa Banatwala, a former masters student in our lab, applied this technique to ISA's. This thesis will compare the results of her work to curvatures calculated analytically from the Legendre polynomials following the method of Kraus (1967).

## PRIOR WORK

Banatwala (2001) acquired input data in the form of serial cross-sectional MRA (magnetic resonance angiography) films from five patients treated at the Malencot Institute at Washington University in St. Louis. The MRA films were photographed with black and white film and then scanned into a computer (Figure 1).

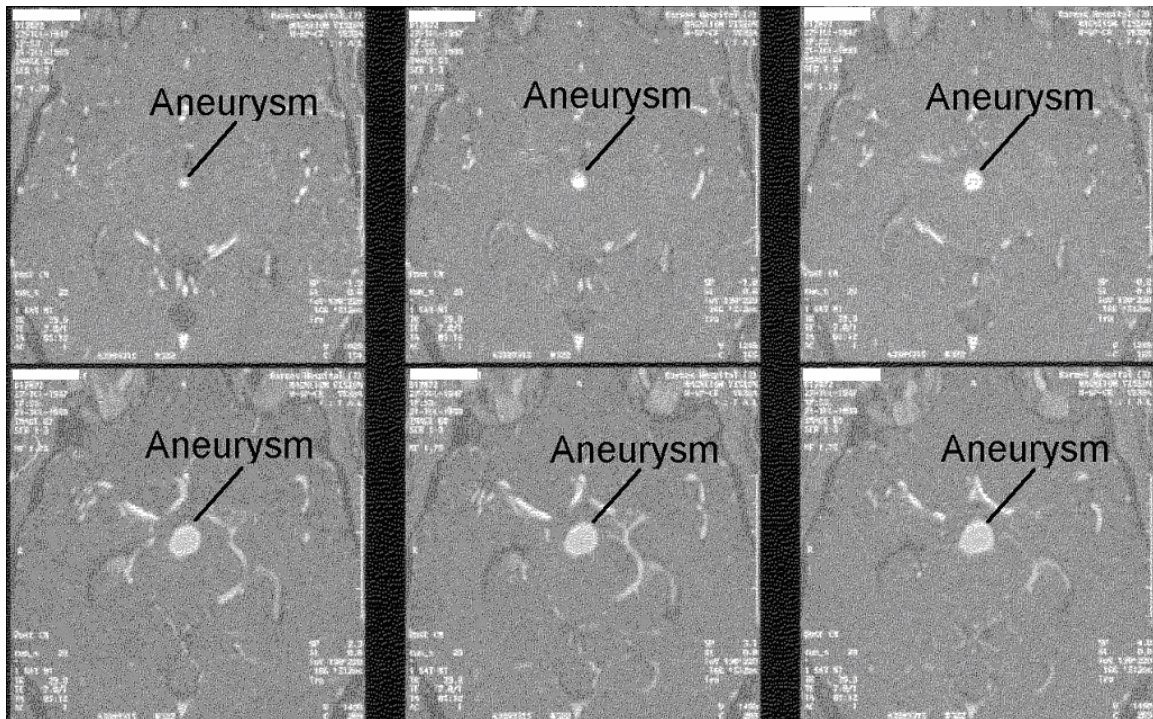
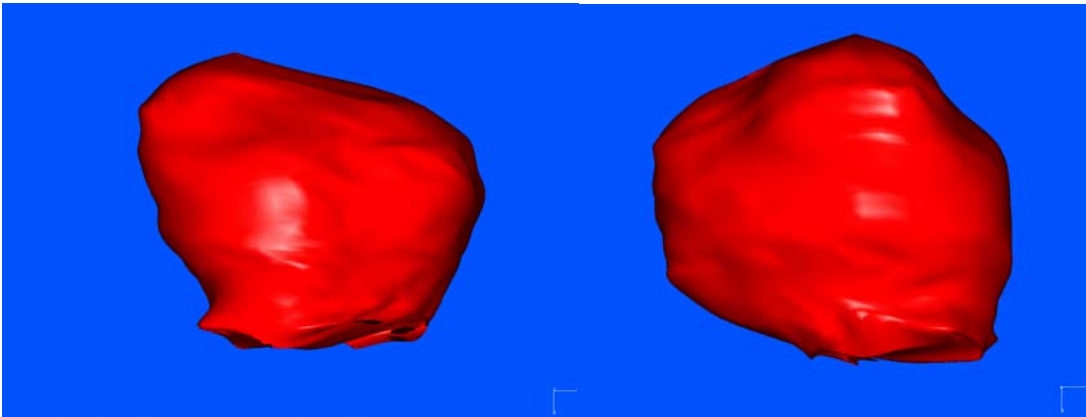


Figure 1. Sample of the MRA images used by Banatwala (2001). From top left to bottom right one sees a sequence of 2-dimensional views in the x-y plane, each separated by 0.9mm in a superior-inferior direction.

The boundaries for these aneurysms were then manually selected and digitized using Scion Image (Scion Corporation, MD). These boundary points effectively define the surface of the aneurysm and allow for the interpolation of remaining points on the surface as well as calculation of specific values for curvature. The digitized surface points were smoothed using local biquadric surface patch (Sacks et al., 1999; Breau et al., 1991) and then read into IDEAS, a solid-modeling package produced by SDRC (Columbus OH). Through the use of splines and a loft procedure within IDEAS, three-dimensional reconstructed surfaces were created (Figure 2).



**Figure 2. Final surface of a human intracranial saccular aneurysm.**

Banatwala then used the splines to try to estimate the local curvatures (Figure 3).

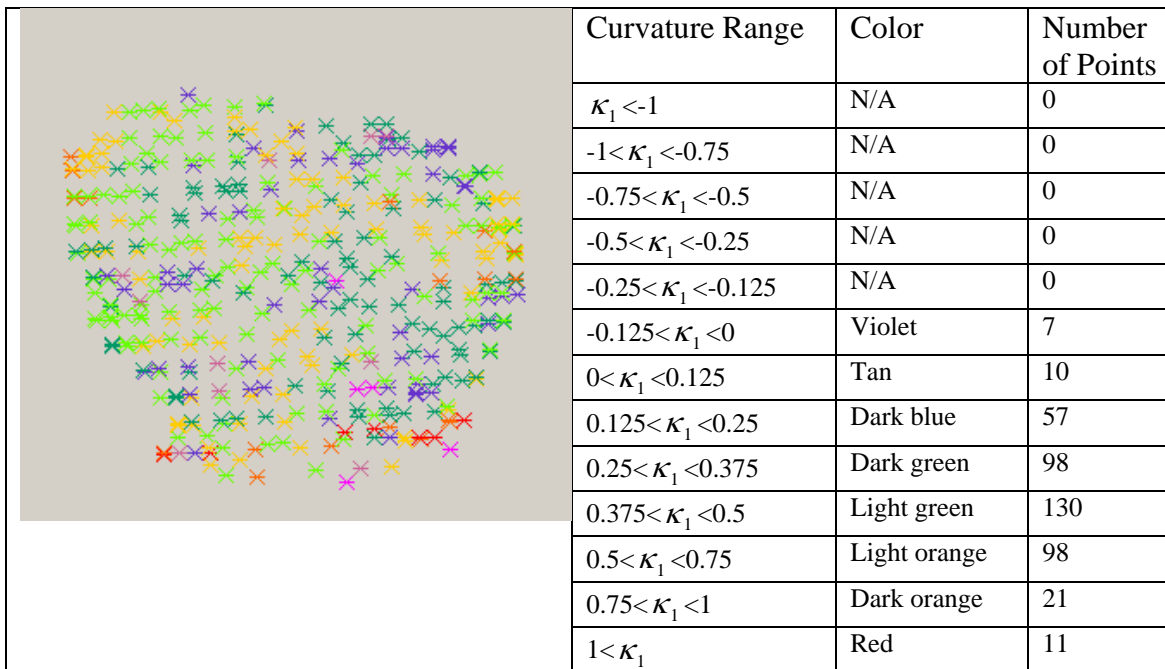


Figure 3. Curvature ( $\kappa_1$ ) values for Aneurysm #3 color-coded by range.

With computation times on the order of ten hours, this method for calculating the curvatures was very time consuming and has a very low feasibility of being used online while the patient is in the MRI machine. In an effort to achieve a reasonable computation time while maintaining as much accuracy as possible, Legendre spheroids were used to estimate the surface of the lesion.

### LEGENDRE POLYNOMIALS

Curvatures can also be calculated given a suitable equation to describe the surface. The often-used assumption is that these lesions can be modeled as truncated

spheres or ellipses and thus, associated equations are used when analyzing idealized lesions. Legendre functions of the first kind, however, are able to provide more accurate descriptions of true aneurysm geometry while still providing an equation that can be fairly easily analyzed. These equations have the added benefit that the shape can be dramatically altered by changing a small number of parameter values. Even in the absence of *in vivo* data, these equations can be used to create idealized versions of several classes of aneurysms for analysis purposes.

### *Legendre Function*

Legendre functions are of the form

$$P_n^m(x) = (-1)^m (1-x^2)^{m/2} \frac{d^m}{dx^m} P_n(x) \quad (6)$$

where  $m$  and  $n$  are integer values,  $P_n(x)$  is a Legendre polynomial, and  $x$  is any argument (Zhang and Jin, 1996). For this research, the boundary of the lesion is described by (Von Seggern, 1990)

$$r = \beta(1 + c \cdot P_n^m(\cos \phi) \cdot \cos(m\theta)) \quad \theta \in [0, 2\pi] \quad \phi \in [0, \pi] \quad (7)$$

where  $r$  is the radius,  $\theta$  and  $\phi$  are angles in spherical coordinates,  $P_n^m$  is the associated Legendre function of the first kind, and  $\beta, c, n$ , and  $m$  are shape parameters. Note that  $\phi$  represents the azimuthal angle. If the center point and the preceding equation for the radius are known, then the shape can be defined at any value of  $\theta$  and  $\phi$ .

To demonstrate the Legendre function, let  $n = 2$  and  $m = 1$ , then the solution to equation 6 is

$$P_2^1(x) = -3x(1-x^2)^{1/2}. \quad (8)$$

Substituting into equation 7 gives

$$r = \beta \left( 1 + c \left( -3(\cos \phi)(1 - \cos^2 \phi)^{1/2} \right) \cdot \cos(m\theta) \right). \quad (9)$$

The Legendre functions were chosen due to their ability to model a wide range of shapes. These shapes range from a simple pear-shape, which could easily be imagined as representative of a somewhat ideal aneurysm, to more complex shapes that more accurately model certain human lesions. Figure 4 demonstrates some of the shapes that can be obtained by varying the values of  $n$  and  $m$ . The left image has values of  $n=3$  and  $m=0$ , the middle image has values of  $n=2$  and  $m=1$ , and the right image has values of  $n=3$  and  $m=1$ .

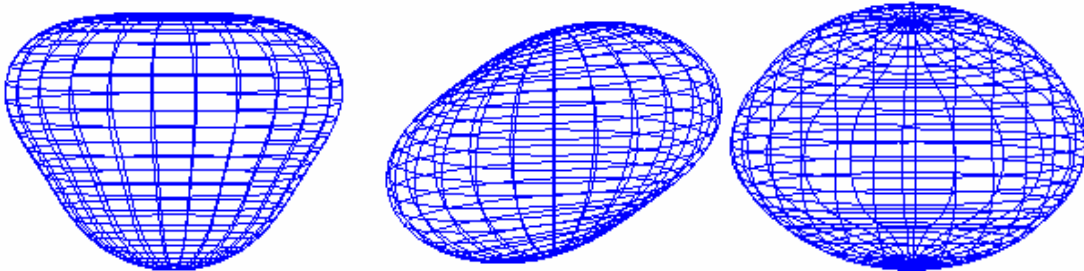


**Figure 4. Variability capable by our chosen function by altering values of  $n$  and  $m$ .**

Varying the value of  $\beta$  will change the overall size of the figure but not the shape.

Varying the value of  $c$  will alter the shape of the figure still further. Figure 5

demonstrates four very different shapes that can be obtained by keeping  $n=3$  and  $m=0$  (see Figure 4-left) while changing the value of  $c$ . Clearly a higher value of  $c$  gives a greater degree of distortion from a spherical geometry.

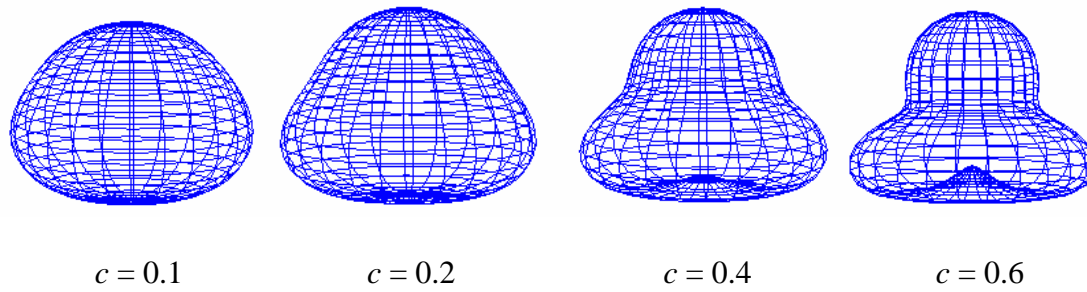


**Figure 5. Effects of varying  $c$  while keeping other parameters constant. ( $n=3, m=0$ )**

The Legendre polynomials were converted from spherical  $(r, \theta, \phi)$  to Cartesian  $(x, y, z)$  coordinates,

$$\mathbf{R} = x\mathbf{i} + y\mathbf{j} + z\mathbf{k}, \quad (10)$$

where

$$\begin{aligned} x &= r \cos \theta \sin \phi \\ y &= r \sin \theta \sin \phi \\ z &= r \cos \phi \end{aligned}$$

and then modified further by multiplying each component by a scalar  $(\alpha x, \gamma y, \delta z)$ ,

$$\mathbf{R} = \alpha x\mathbf{i} + \gamma y\mathbf{j} + \delta z\mathbf{k}, \quad (11)$$

effectively stretching the spheroid in the three orthogonal directions.

The objective was to minimize the difference between the actual radius calculated from the MRA data at each point and the radius calculated from the Legendre-based function. A Marquardt-Levenberg regression code written in MATLAB (see Appendix 3) was employed to determine those parameter values that minimized the sum of squares error (SSE), namely

$$SSE = \sum (r - r_{th})^2 . \quad (12)$$

The parameters used to minimize this error were the shape parameters  $m, n, c, \alpha, \gamma, \delta$ , the size parameter  $\beta$ , the location parameters  $x_0, y_0, z_0$ , and the orientation parameters  $rot1, rot2, rot3$ . Once again,  $m, n$  define the Legendre polynomial,  $c$  determines the amount of perturbation from a sphere,  $\alpha, \gamma, \delta$  are the stretches in the  $x, y$ , and  $z$  directions respectively and  $\beta$  merely enlarges the spheroid without affecting the shape. The three parameters  $x_0, y_0$ , and  $z_0$  define the location of the center of the spheroid, and  $rot1, rot2$ , and  $rot3$  are the Euler angles for the rigid rotation of a 3-D shape. The mean squared error (MSE),

$$MSE = \frac{SSE}{N} , \quad (13)$$

was used as the measure of fit by defining the root mean squared error (RMS) as

$$RMS = \sqrt{MSE} , \quad (14)$$

where  $N$  is the number of data points. Note that the values for RMS have the units of millimeters (mm).

## METHODS

The input data from the serial cross-sectional MRA films from five patients was studied using the MATLAB code and a Legendre spheroid was defined for each of the five aneurysms.

Once a Legendre spheroid fits the data (i.e. models the aneurysm), curvatures can be calculated analytically using standard computations. Once again, consider a Legendre function  $P_n^m$  and a spheroid of radius,  $r$ , and  $\beta = 1$  given by

$$r = 1 + cP_n^m(\cos \phi)\cos(m\theta) \quad (15)$$

where  $c$  is an arbitrary constant. Referring the spherical surface  $(r, \theta, \phi)$  to Cartesian coordinates  $(x, y, z)$ , the surface can be defined to be

$$\mathbf{R} = r \sin \phi \cos \theta \mathbf{i} + r \sin \phi \sin \theta \mathbf{j} + r \cos \phi \mathbf{k}. \quad (16)$$

An infinitesimal movement on the surface can be described by

$$d\mathbf{R} = \mathbf{R}_{,\theta} d\theta + \mathbf{R}_{,\phi} d\phi, \quad (17)$$

where  $\mathbf{R}_{,\theta}$  and  $\mathbf{R}_{,\phi}$  are the base vectors defined by

$$\mathbf{R}_{,\theta} = \frac{\partial \mathbf{R}}{\partial \theta}, \text{ and } \mathbf{R}_{,\phi} = \frac{\partial \mathbf{R}}{\partial \phi}, \quad (18)$$

which are easily computed from equations 10 and 11. Hence,

$$\begin{aligned} \mathbf{R}_{,\theta} = & \left( \frac{\partial r}{\partial \theta} \sin \phi \cos \theta - r \sin \phi \sin \theta \right) \mathbf{i} + \left( \frac{\partial r}{\partial \theta} \sin \phi \sin \theta + r \sin \phi \cos \theta \right) \mathbf{j} \\ & + \frac{\partial r}{\partial \theta} \cos \phi \mathbf{k}, \end{aligned} \quad (19)$$

and

$$\begin{aligned} \mathbf{R}_{,\phi} = & \left( \frac{\partial r}{\partial \phi} \sin \phi \cos \theta + r \cos \phi \cos \theta \right) \mathbf{i} + \left( \frac{\partial r}{\partial \phi} \sin \phi \sin \theta + r \cos \phi \sin \theta \right) \mathbf{j} \\ & + \left( \frac{\partial r}{\partial \phi} \cos \phi - r \sin \phi \right) \mathbf{k}, \end{aligned} \quad (20)$$

where

$$\frac{\partial r}{\partial \theta} = -cP_n^m(\cos \phi)m \sin(m\theta), \text{ and } \frac{\partial r}{\partial \phi} = c \frac{\partial P_n^m(\cos \phi)}{\partial \phi} \cos(m\theta). \quad (21)$$

Next, define  $dS$  to be the magnitude of the vector  $d\mathbf{R}$ . Squaring  $dS$  yields the first fundamental form

$$dS^2 = d\mathbf{R} \cdot d\mathbf{R} = E(d\theta)^2 + 2Fd\theta d\phi + G(d\phi)^2, \quad (22)$$

where  $E$ ,  $F$ , and  $G$  are defined as

$$E = \mathbf{R}_{,\theta} \cdot \mathbf{R}_{,\theta}, \quad F = \mathbf{R}_{,\theta} \cdot \mathbf{R}_{,\phi}, \quad \text{and } G = \mathbf{R}_{,\phi} \cdot \mathbf{R}_{,\phi}. \quad (23)$$

The unit normal vector to the surface,  $\mathbf{n}$ , can be found using

$$\mathbf{n} = \frac{\mathbf{R}_{,\theta} \times \mathbf{R}_{,\phi}}{|\mathbf{R}_{,\theta} \times \mathbf{R}_{,\phi}|} = \frac{\mathbf{R}_{,\theta} \times \mathbf{R}_{,\phi}}{\sqrt{EG - F^2}}. \quad (24)$$

The curvature vector  $\mathbf{k}$  is given by  $d\mathbf{t}/ds$  where  $\mathbf{t}$  is the unit tangent vector. Dividing  $\mathbf{k}$  into its components yields

$$\mathbf{k} = \frac{d\mathbf{t}}{dS} = \mathbf{k}_n + \mathbf{k}_t, \quad (25)$$

where  $\mathbf{k}_n$  and  $\mathbf{k}_t$  are the normal and tangential components of the curvature vector, or the normal curvature vector and the tangential curvature vector, respectively. For the purposes of this paper, only the normal curvature is considered. Since  $\mathbf{k}_n$  is normal to the surface, it is proportional to  $\mathbf{n}$  by

$$\mathbf{k}_n = -K_n \mathbf{n}, \quad (26)$$

where  $K_n$  is called the normal curvature. Since  $\mathbf{n}$  and  $\mathbf{t}$  are perpendicular,  $\mathbf{n} \cdot \mathbf{t} = 0$ . Taking the derivative with respect to  $S$  yields

$$\frac{d\mathbf{n}}{dS} \cdot \mathbf{t} + \frac{d\mathbf{t}}{dS} \cdot \mathbf{n} = 0. \quad (27)$$

Combining these yields a definition for  $K_n$ ,

$$K_n = \frac{d\mathbf{R} \cdot d\mathbf{n}}{d\mathbf{R} \cdot d\mathbf{R}}. \quad (28)$$

Note that  $d\mathbf{n}$  can be described by  $d\mathbf{n} = \mathbf{n}_{,\theta}d\theta + \mathbf{n}_{,\phi}d\phi$  and recall  $d\mathbf{R} = \mathbf{R}_{,\theta}d\theta + \mathbf{R}_{,\phi}d\phi$ .

Using these relationships,  $K_n$  can now be computed as (Kraus, 1967)

$$K_n = \frac{L(d\theta)^2 + 2Md\theta d\phi + N(d\phi)^2}{E(d\theta)^2 + 2Fd\theta d\phi + G(d\phi)^2}, \quad (29)$$

where  $L$ ,  $M$ , and  $N$  are second fundamental magnitudes given by

$$L = \mathbf{R}_{,\theta} \cdot \mathbf{n}_{,\theta} = -\mathbf{R}_{,\theta\theta} \cdot \mathbf{n},$$

$$M = \frac{1}{2}(\mathbf{R}_{,\theta} \cdot \mathbf{n}_{,\phi} + \mathbf{R}_{,\phi} \cdot \mathbf{n}_{,\theta}) = -\mathbf{R}_{,\theta\phi} \cdot \mathbf{n}, \quad (30)$$

$$\text{and} \quad N = \mathbf{R}_{,\phi} \cdot \mathbf{n}_{,\phi} = -\mathbf{R}_{,\phi\phi} \cdot \mathbf{n},$$

where  $\mathbf{R}_{,\theta\theta}$ ,  $\mathbf{R}_{,\phi\phi}$ ,  $\mathbf{R}_{,\theta\phi}$  are

$$\mathbf{R}_{,\phi\phi} = \frac{\partial^2 \mathbf{R}}{\partial \phi^2}, \quad \mathbf{R}_{,\theta\theta} = \frac{\partial^2 \mathbf{R}}{\partial \theta^2}, \quad \text{and} \quad \mathbf{R}_{,\theta\phi} = \frac{\partial^2 \mathbf{R}}{\partial \theta \partial \phi}. \quad (31)$$

The principal curvatures are the maximum or minimum values of  $K_n$ . Define the direction to be  $\lambda = d\phi/d\theta$  and  $K_n$  becomes

$$K_n(\lambda) = \frac{L + 2M\lambda + N\lambda^2}{E + 2F\lambda + G\lambda^2}. \quad (32)$$

The normal curvature reaches a maximum or minimum where  $dK_n/d\lambda = 0$  or

$$0 = (E + 2F\lambda + G\lambda^2)(M + N\lambda) - (L + 2M\lambda + N\lambda^2)(F + G\lambda). \quad (33)$$

Reducing yields

$$(E + F\lambda)(M + N\lambda) = (F + G\lambda)(L + M\lambda), \quad (34)$$

or

$$0 = (MG - NF)\lambda^2 + (LG - NE)\lambda + (LF - ME), \quad (35)$$

and using the quadratic equation  $\lambda$  becomes

$$\{\lambda_1, \lambda_2\} = \frac{-(LG - NE) \pm \sqrt{(LG - NE)^2 - 4(MG - NF)(LF - ME)}}{2(MG - NF)}, \quad (36)$$

where  $\lambda_1$  and  $\lambda_2$  are the directions of the principal curvatures. Substituting them into

Equation 27 yields the principal curvatures

$$\kappa_1 \equiv (K_n)_1 = \frac{L + 2M\lambda_1 + N\lambda_1^2}{E + 2F\lambda_1 + G\lambda_1^2} \quad \text{and} \quad \kappa_2 \equiv (K_n)_2 = \frac{L + 2M\lambda_2 + N\lambda_2^2}{E + 2F\lambda_2 + G\lambda_2^2}. \quad (37)$$

## RESULTS

Banatwala (2001) was able to generate an improvement on the MSE of approximately 30% over the current standard of the sphere by using an unmodified Legendre spheroid. By modifying the Legendre function via scalar multiples in the primary coordinate directions, this research was able to generate a further improvement of 1 to 11%. This improvement totals from 26 to 170% over the sphere for the five lesions modeled. Table 1 shows the parameter values for each of the 5 lesions. The first column shows the values obtained by Banatwala's genetic search algorithm, the second column displays the values obtained by the current Marquardt-Levenberg search algorithm for an unmodified Legendre spheroid, and the final column displays the values obtained by for a modified Legendre spheroid.

The curvature values for all five lesions are shown in graphical form in the appendix. For Aneurysm #3, the modified Legendre spheroids are shown in figures 6 and 7 with the values for the curvatures mapped onto the surface and delineated by color.

Table 1: Tabulated results from the various modeling methods.

	Aneurysm #1			Aneurysm #2			Aneurysm #3		
	Prior	Unmodified	Modified	Prior	Unmodified	Modified	Prior	Unmodified	Modified
<b>c</b>	0.28	0.29	0.0099	0.22	0.9421	0.0231	0.06	0.1174	0.0116
<b>beta</b>	4.03	4.01	2.1185	6.53	5.79	3.3539	3.99	4	2.19
<b>m</b>	1	1	2	0	0	0	1	1	0
<b>n</b>	2	2	4	2	1	3	2	2	3
<b>alpha</b>	x	1	1.71	x	1	2.1948	x	1	1.8
<b>gamma</b>	x	1	2.63	x	1	2.4612	x	1	1.48
<b>delta</b>	x	1	1.17	x	1	1.7276	x	1	2.13
<b>xo</b>	64.36	0.08	0.03	65.09	-2.41	-0.03	25.97	-0.03	0.065
<b>yo</b>	38.46	0.09	-0.1044	61.79	-3.2	-0.25	31.32	-0.11	-0.074
<b>zo</b>	-18.86	0.06	0.0476	5.5	3.45	-0.1133	3.87	-0.04	-0.041
<b>rot1</b>	0.5824	-1.3	0.7055	2.5831	0.83	-0.0063	2.4817	-1.58	-0.78
<b>rot2</b>	3.4477	-1.47	0.025	3.2463	0.1679	-0.0777	0.0466	-1.36	-0.02
<b>rot3</b>	2.2759	-1.15	-1.75	2.1468	-0.8558	-0.0628	3.8094	0.866	-1.53
<b>RMS (mm)</b>	0.4083	0.4015	0.3667	0.4821	0.4599	0.4217	0.2764	0.2653	0.2625
<b>improv. over unmodified</b>			9.48%			9.07%			1.08%

	Aneurysm #4			Aneurysm #5		
	Prior	Unmodified	Modified	Prior	Unmodified	Modified
<b>c</b>	0.16	0.1172	0.1582	0.57	2.11	0.1097
<b>beta</b>	10.74	10.38	3.42	2.75	1.84	1.71
<b>m</b>	0	0	0	0	0	0
<b>n</b>	4	4	4	2	1	4
<b>alpha</b>	x	1	3.04	x	1	2.6928
<b>gamma</b>	x	1	3.39	x	1	2.2223
<b>delta</b>	x	1	2.86	x	1	1
<b>xo</b>	15.36	-0.69	0.0867	53.52	-2.96	-0.0366
<b>yo</b>	13.12	1.07	-0.533	39.65	2	-0.1095
<b>zo</b>	30.87	-0.1178	-0.325	36.03	1.21	-0.1564
<b>rot1</b>	2.2864	-2.49	-0.3589	3.3859	-5.04	-0.0143
<b>rot2</b>	5.4978	-5.13	-0.4586	5.5501	-5.76	-0.472
<b>rot3</b>	0.8901	-3.89	1.71	1.1345	-5.7	-0.7619
<b>RMS (mm)</b>	0.8727	0.8707	0.8123	0.2975	0.3180	0.2853
<b>improv. over unmodified</b>			7.18%			11.45%

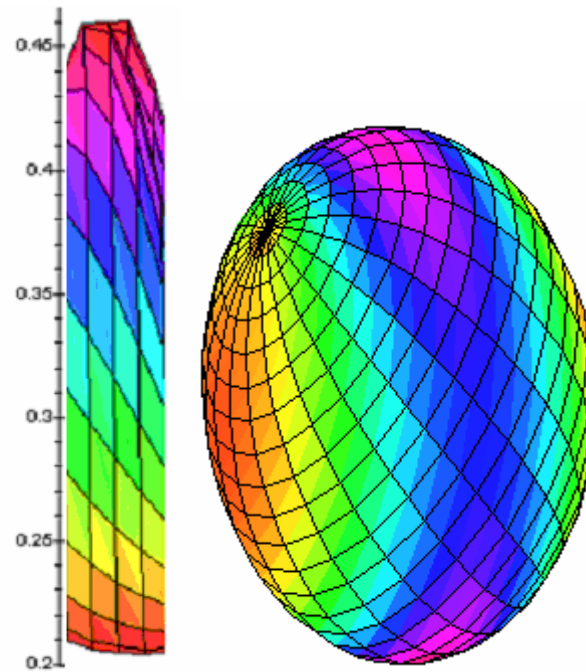


Figure 6: For Aneurysm 3, the values of the maximum curvature values.  $\kappa_1$ , range from 0.2 to 0.46.

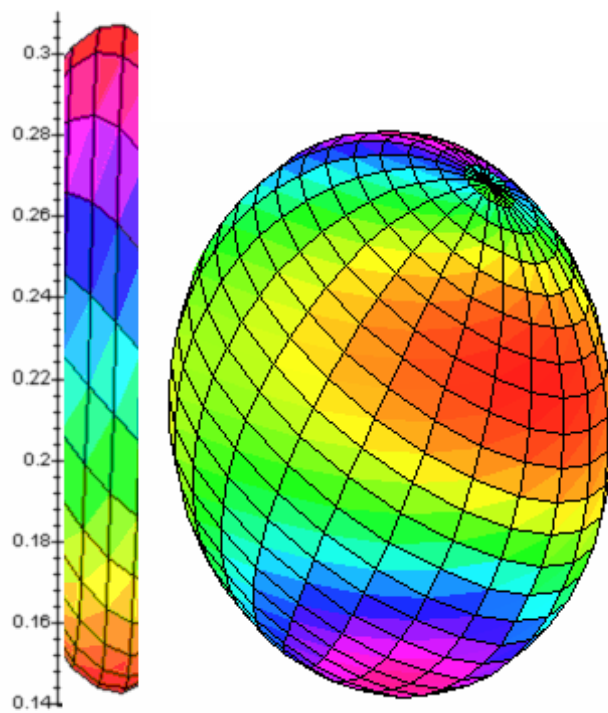
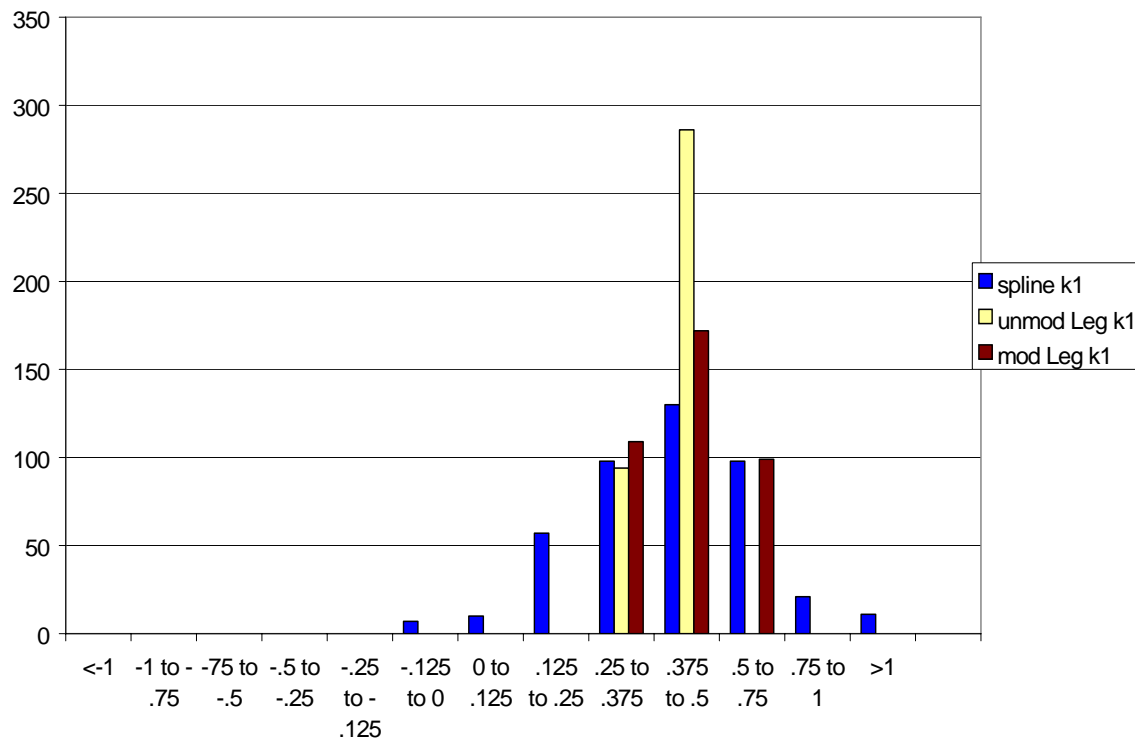
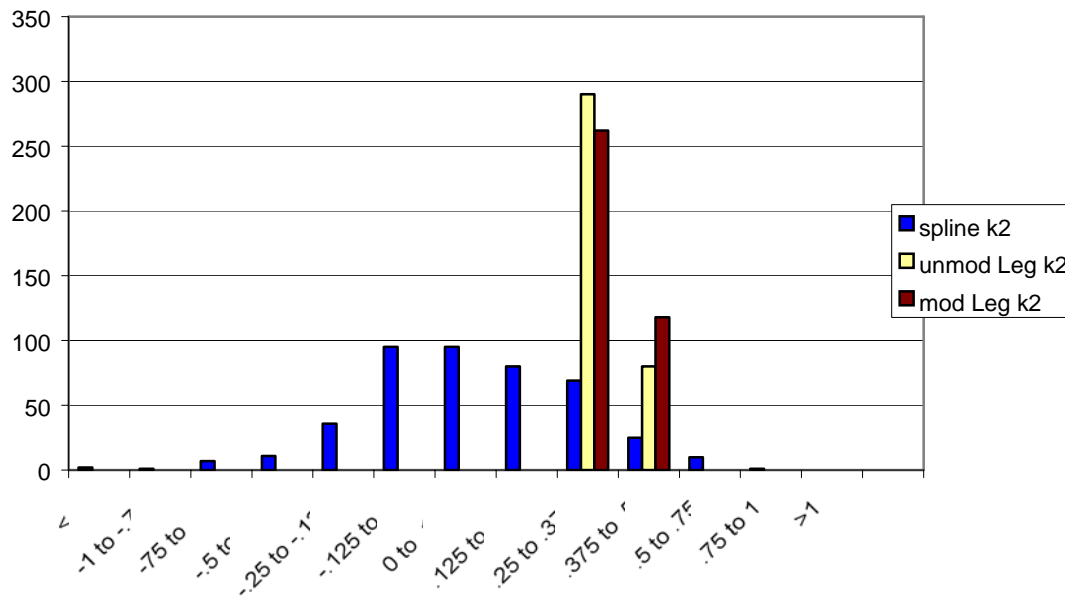


Figure 7: For Aneurysm 3, the values of the minimum curvature values.  $\kappa_2$ , range from 0.14 to 0.32.

For comparison, a histogram of the curvatures found by each of the three methods is shown for Aneurysm #3 in figures 8 and 9 below.



**Figure 8: Aneurysm 3 Kappa 1.**



**Figure 9: Aneurysm 3 Kappa 2.**

Finally, Table 2 lists the computation times in seconds for each of the 5 lesions. Note that the genetic algorithm used by Banatwala (2001) required ten hours, not seconds, of computing time.

**Table 2: Computation times for modified and unmodified Legendre spheroids.**

	Plot		Curvatures		Total	
	Unmodified	Modified	Unmodified	Modified	Unmodified	Modified
1	1.5	39	2	87	3.5	126
2	2.2s	7.5	6s	35	8.2s	42.5
3	1.6	8.4	7.5	50	9.1	58.4
4	4s	9.6s	24s	1.7	28s	1.9
5	2.4s	12s	3s	11s	5.4s	23s

## DISCUSSION

Saccular aneurysms have long been approximated as spheres for the sake of simplicity (Scott et al., 1972; Canham and Ferguson, 1985; Humphrey and Kryiacou 1996; Chitanvis et al. 1997; Shah and Humphrey 1999). Given this approximation, we have obtained some useful information, yet due to the membrane-like character, we know that regional curvatures are key (Shah et. al., 1997). Indeed, as early as 1962, geometry and location were considered important in discerning the risk of rupture (Crompton, 1962; Ujiie et. al., 1993). Ujiie et al. (1999) claimed further that aneurysms with a ratio of maximum dimension to minimum dimension greater than 1.6 should be treated regardless of diameter. In hindsight, the common neglect of shape (curvatures) has resulted, in part, in the controversy over a critical size, and its neglect explains in part the finding by the international study on unruptured intracranial saccular aneurysms (ISUIA) that size in no way predicts risk of rupture in lesions less than 10mm in diameter (Weibers, 1998). Consideration of shape and, in particular, curvatures rather than maximum dimension, implies the need for a more accurate descriptor than the default spherical shape for an aneurysm. By modeling aneurysms with more complicated shapes using Legendre spheroids, we are now able to begin to estimate the curvature at specific locations on a lesion. The average *RMS* values were 0.47 mm for the standard Legendre function and 0.81 mm for the sphere for a 43% improvement. By modifying the Legendre spheroid, we were able to further improve the *RMS* by another 1 to 11%. This percentage may not seem drastic, but the curvatures for Aneurysm #3, which showed the 1% improvement, changed by as much as 35% for  $\kappa_1$ . This 35% change has a significant impact on the

stress of the membrane (see equation 3). RMS values for the modified Legendre spheroid were still relatively high at 0.26 to 0.8mm when compared to current MR resolution at 0.2 mm; this suggests that there is still improvement needed for the analytical model to fully exploit current technology.

Non-conforming surface patches based on splines have a tendency to create anomalies that can be misleading for understanding the characteristic shapes of the aneurysm. Conversely, the Legendre spheroids smooth the surface, which can result in the removal of certain features that may be important in understanding the true nature of the aneurysm. A comparison between the Legendre spheroid and splines in Figure 8 shows the mean value of the maximum curvatures ( $\kappa_1$ ) correspond well; however, the curvature values for the Legendre spheroid have a smaller variance due to the smoothing effects. In Figure 9, the mean value of the minimum curvatures ( $\kappa_2$ ) compare less favorably. The Legendre spheroid has positive curvatures throughout, while the spline fit has a large number of negative curvatures as well. Viewing the reconstruction of the lesion by eye, there are some major features that seem like they should produce some negative curvatures, but not on the scale that the spline fit produces. The increased number of negative curvatures may be a result of the undulations induced by the spline fitting. The function chose to fit the data has a significant impact on the shape and error produced. We chose Legendre spheroids because of their simplicity, but more complex functions can be used to gain higher degrees of accuracy. In the future, therefore, we should seek generalizations of equation 10 or other classes of functions.

Time is another major factor in deciding which model would be most appropriate to use for modeling a lesion. The current standard of a sphere would require a search for only one parameter, the radius, which would result in basically zero computation time. Modifying the sphere by means of a Legendre polynomial decreases the RMS error by 15 to 61% and increases the computation time to 2.7 minutes. Further modification by multiplying each of the three Cartesian directions by a scalar reduces the RMS error by another 1 to 11% for a total improvement of 26 to 170% over the sphere. Computation times are increased by an order of magnitude, however, to an average of 45 minutes. The surface patch technique, which seems to be the safest estimate, increases computation time by another order of magnitude to 10 hours.

## CONCLUSIONS

Advances in vascular biology reveal a ubiquitous sensitivity of vascular cells (endothelial, smooth muscle, and fibroblasts) to even slight changes in their mechanical environment. In response to such changes, cells alter their production of vasoactive molecules, growth factors, cytokines, and proteases as well as their synthesis of matrix. Such changes likely control the growth and remodeling of saccular aneurysms and thereby likely control the rates and extent of enlargement as well as their rupture-potential (Ryan and Humphrey, 1999). There is a need, therefore, to track better the regional multi-axial mechanical stresses. Because of their membrane character, the stresses in saccular aneurysms are likely governed in large part by regional curvatures, which are potentially measurable by combining surface-fitting techniques with advances in clinical imaging such as MRA. We have shown that a modified Legendre polynomial representation of lesion shape can be obtained from clinical data and that it yields a marked improvement over the status quo, the maximum dimension based on a spherical template. There is a need, however, for further research to explore other analytically tractable functions to improve further our ability to assess aneurysmal shape in vivo.

## REFERENCES

Banatwala M., 2001, Computational Analysis and the Geometry of Intracranial Saccular Aneurysms, Master of Science thesis, Department of Biomedical Engineering, Texas A&M University, College Station.

Breau, C., Shirazi-Adl, A., de Guise, J., 1991. Reconstruction of a human ligamentous lumbar spine using CT images – A three-dimensional finite element mesh generation. *Annals of Biomedical Engineering* 19, 291-302.

Canham, P.B., Ferguson, G.G., 1985. A mathematical model for the mechanics of saccular aneurysms. *Neurosurgery* 17(2), 291-5.

Canham, P.B., Finlay, H.M., Kiernan, J.A., Ferguson, G.G., 1999. Layered structure of saccular aneurysms assessed by collagen birefringence. *Neurological Research*. 21, 618-626.

Chitanvis S.M., Dewey M., Hademenos G., Powers W.J., Massoud T.F., 1997. A nonlinear quasi-static model of intracranial aneurysms. *Neurological Research*. 19(5), 489-96.

Crompton M.R. 1962. The pathology of ruptured middle-cerebral aneurysms with special reference to the difference between the sexes. *The Lancet*. 421-425.

Crompton, M.R., 1966. Mechanism of growth and rupture in cerebral berry aneurysms, *British Journal of Neurosurgery* 1, 1138-1142.

Dorland's Illustrated Medical Dictionary, 1996. Saunders, Philadelphia

Elger, D.F., Blackketter, D.M., Budwig, R.S., Johansen, K.H., 1996. The influence of shape on the stresses in model abdominal aortic aneurysms. *Transactions of the ASME* 118, 326-332.

Hademenos, G.J., Massoud, T.F., Turjman, F., Sayre, J.W. 1998. Anatomical and morphological factors correlating with rupture of intracranial aneurysms in patients referred for endovascular treatment. *Neuroradiology* 40, 755-760.

Humphrey, J.D. and Kyriacou, S.K. 1996 The use of Laplace's equation in aneurysm mechanics. *Neurol Res* 18, 204-208.

Humphrey, J.D., 1998. Computer methods in membrane biomechanics. *Computer Methods in Biomechanics and Biomedical Engineering* 1, 171-210.

Kraus, H., 1967. *Thin Elastic Shells An Introduction to the Theoretical Foundations and the Analysis of Their Static and Dynamic Behavior*. John Wiley & Sons, New York.

Mimata, C., Kitaoka, M., Nagahiro, S., Iyama, K., Hori, H., Yoshioka H., Ushio, Y., 1997. Differential distribution and expressions of collagens in the cerebral aneurysmal wall. *Acta Neuropathologica* 94, 197-206.

Orz, Y., Kobayashi, S., Osawa, M., Tanaka, Y., 1997. Aneurysm size: a prognostic factor for rupture. *British Journal of Neurosurgery* 11(2), 144-149.

Parlea, L., Fahrig, R., Holdsworth D.W., and Lownie, S.P. (1999) An analysis of the geometry of saccular intracranial aneurysms. *Am J Neuroradiol* 20, 1079-1089.

Ryan, J.M., Humphrey, J.D., 1999. Finite element based predictions of preferred material symmetries in saccular aneurysms. *Annals of Biomedical Engineering* 27, 641-647.

Sacks, M.S., Vorp, D.A., Raghavan, M.L., Federle, M.P., Webster, M.W., 1999. In vivo three-dimensional surface geometry of abdominal aortic aneurysms. *Annals of Biomedical Engineering* 27, 469-479.

Scott, S., Ferguson, G.G., Roach, M.R., 1972. Comparison of the elastic properties of human intracranial arteries and aneurysms. *Can J Physiol Pharmacol* 50(4),328-32.

Shah, A.D., Harris, J.L., Kyriacou, S.K., Humphrey, J.D., 1997. Further roles of geometry and properties in saccular aneurysm mechanics. *Computer Methods in Biomechanics and Biomedical Engineering* 1, 109-121.

Shah, A.D., Humphrey, J.D., 1999. Finite strain elastodynamics of intracranial saccular aneurysms. *Journal of Biomechanics* 32(6), 593-9.

Ujiie, H., Sato, K., Onda, H., Oikawa, A., Kagawa, M., Takakura, K., Kobayashi N., 1993. Clinical analysis of incidentally discovered unruptured aneurysms. *Stroke* 24, 1850-1856.

Ujiie, H., Tachibana, H., Hiramatsu, O., Hazel, A.L., Matsumoto, T., Ogasawara, Y., Nakajima, H., Hori, T., Takakura, K., Kajiya, F., 1999. Effects of size and shape (aspect ratio) on the hemodynamics of saccular aneurysms: a possible index for surgical treatment of intracranial aneurysms. *Neurosurgery* 45(1),119-29; discussion 129-30.

Von Seggern, D.H., 1990. CRC Handbook of Mathematical Curves and Surfaces. CRC Press, Boca Raton, FL.

Vorp, D., Raghavan, M., Webster, M., 1998. Mechanical wall stress in abdominal aortic aneurysm: influence of diameter and asymmetry. *Journal of Vascular Surgery* 27(3), 632-639.

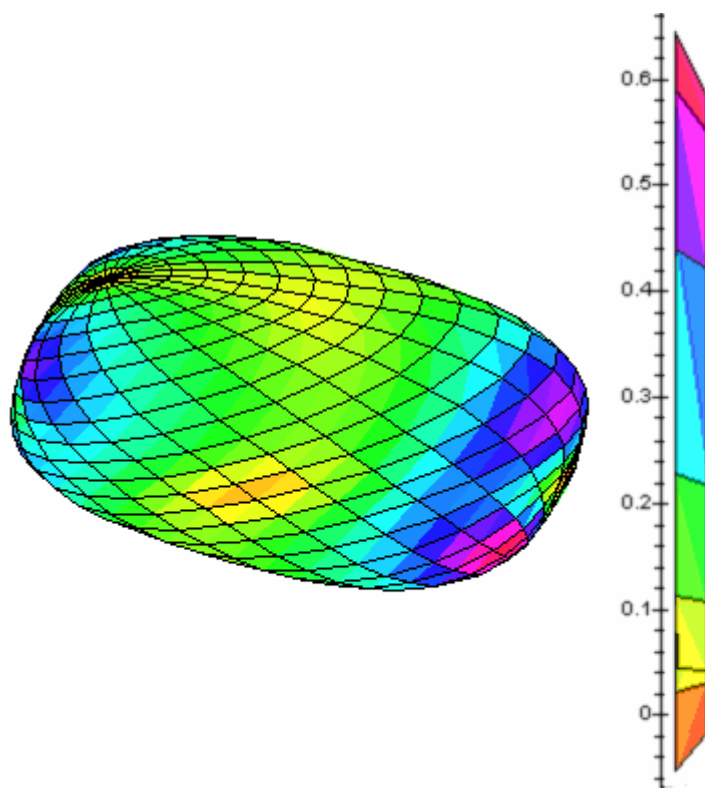
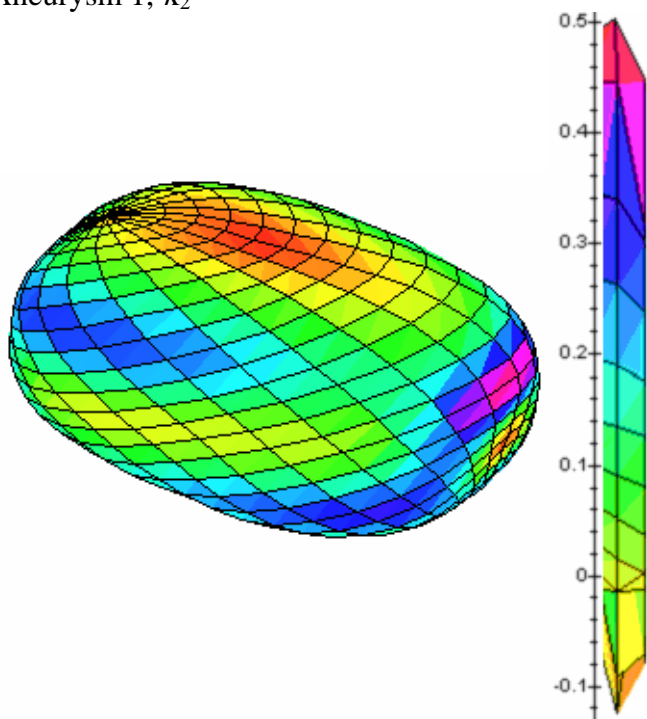
Wiebers, D.O., 1998. Unruptured intracranial aneurysms – risk of rupture and risks of surgical intervention. *The New England Journal of Medicine* 339, 1725-1733.

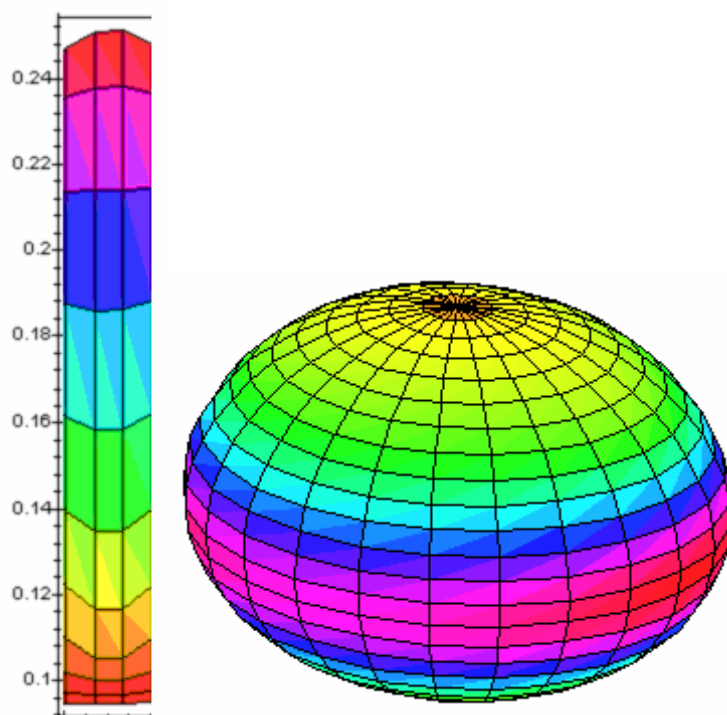
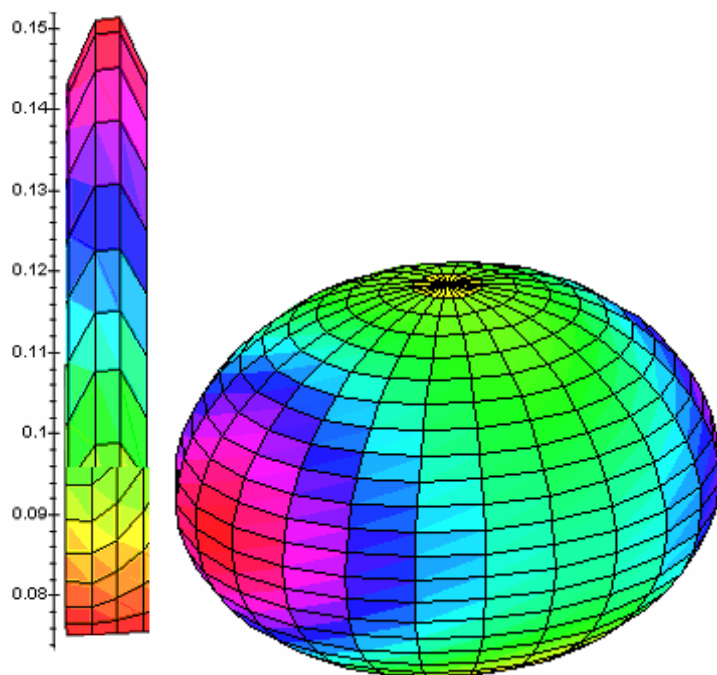
Zacks, D.J., Russell, D.B., Miller, J.D.R., 1980. Fortuitously discovered intracranial aneurysms. *Arch Neurologica* 37, 39-41.

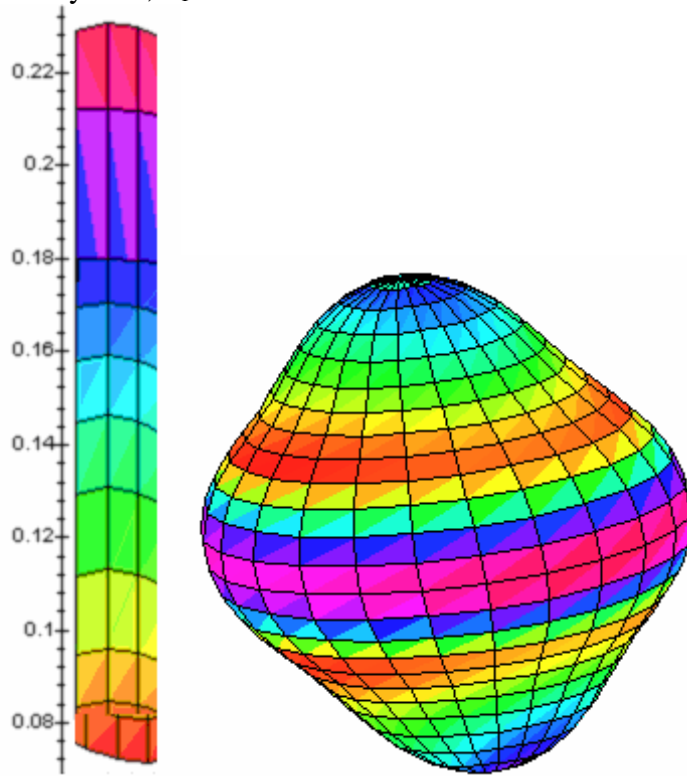
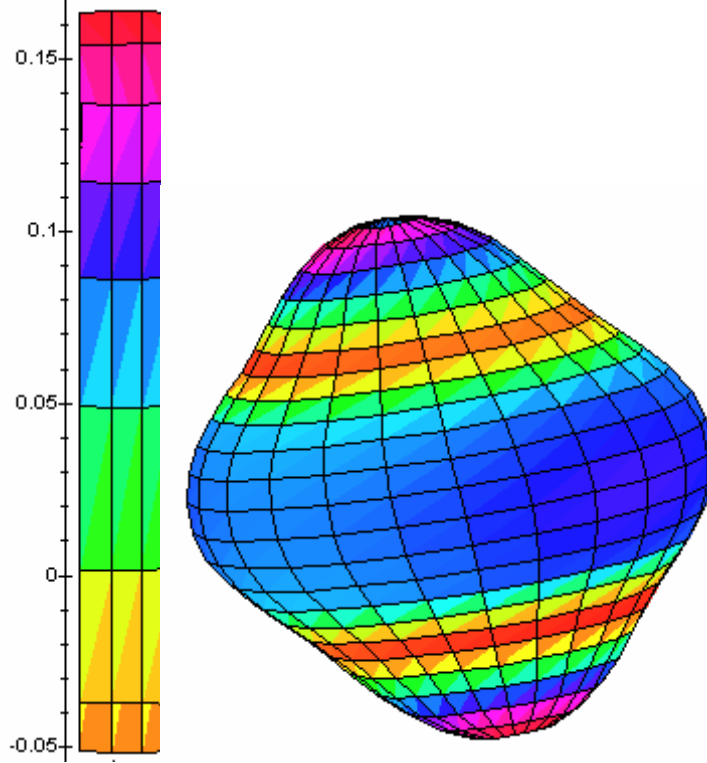
Zhang, S., Jin, J., 1996. *Computation of Special Functions*. John Wiley & Sons, Inc., New York.

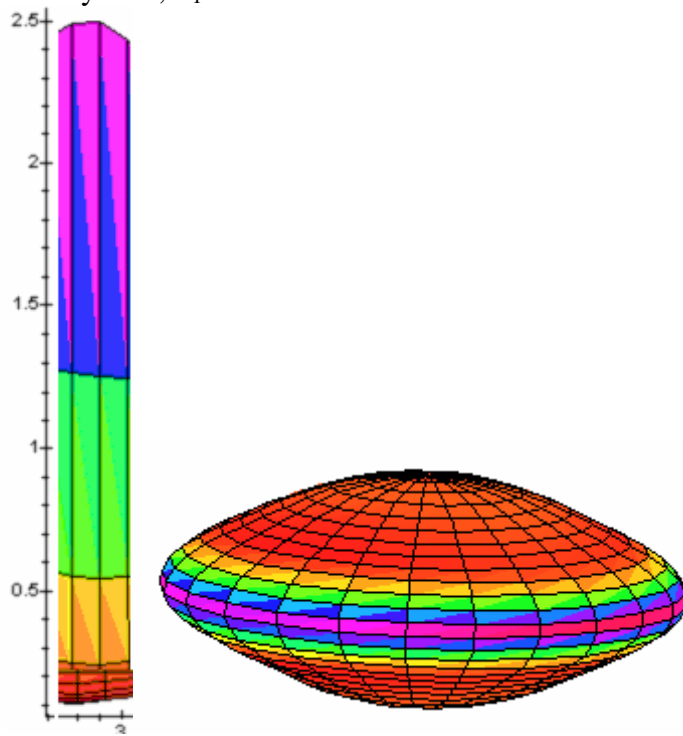
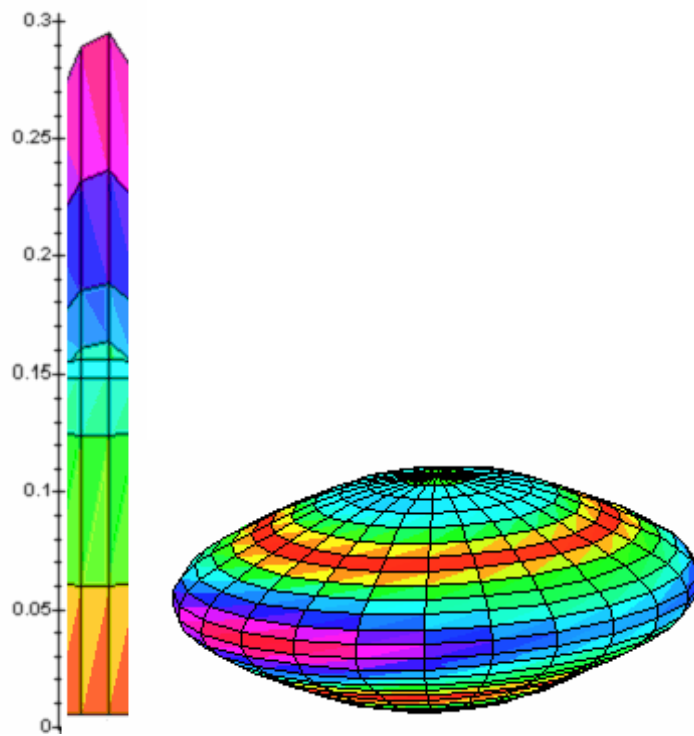
## APPENDIX 1

The reconstruction of the other four digitized aneurysms are shown with the curvature values mapped on the surface by color. Each aneurysm is shown with the maximum ( $\kappa_1$ ) and minimum ( $\kappa_2$ ) curvature values.

Aneurysm 1,  $\kappa_1$ Aneurysm 1,  $\kappa_2$ 

Aneurysm 2,  $\kappa_1$ Aneurysm 2,  $\kappa_2$ 

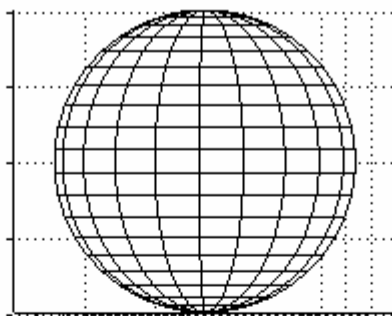
Aneurysm 4,  $\kappa_1$ Aneurysm 4,  $\kappa_2$ 

Aneurysm 5,  $\kappa_1$ Aneurysm 5,  $\kappa_2$ 

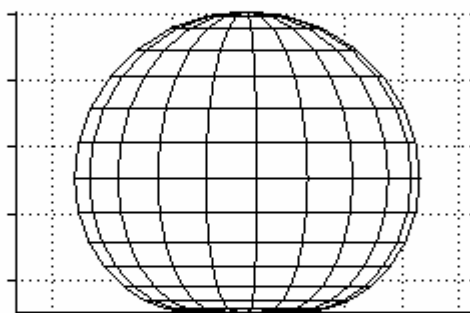
## **APPENDIX 2**

A catalog of unmodified Legendre spheroids is presented giving an idea of the variety of shapes that can be created with this method and how each parameter affects the spheroid.

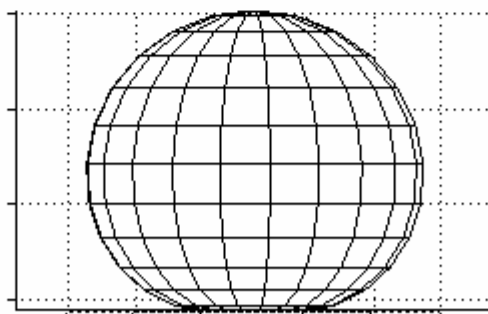
$$m=0 \quad n=1$$



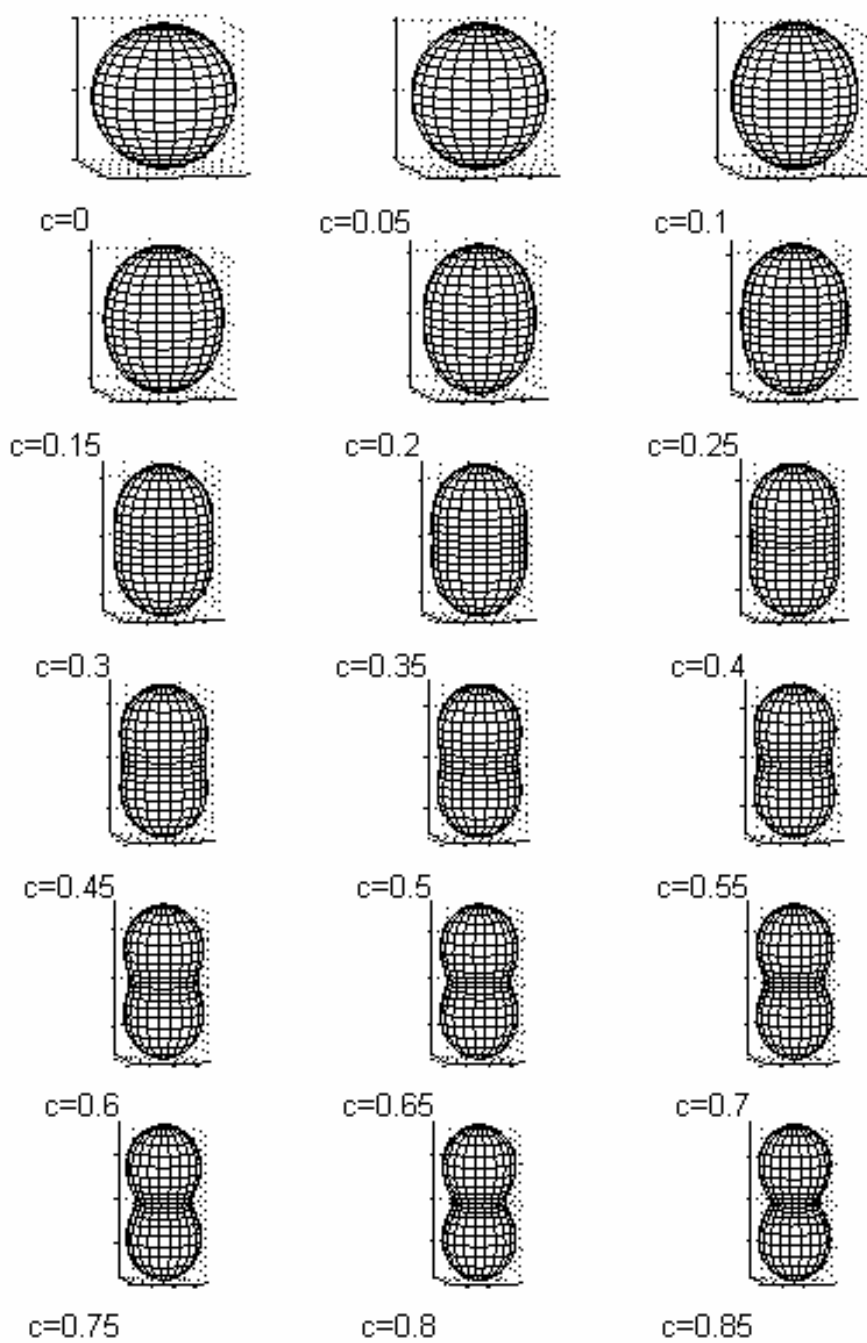
$$c=0$$

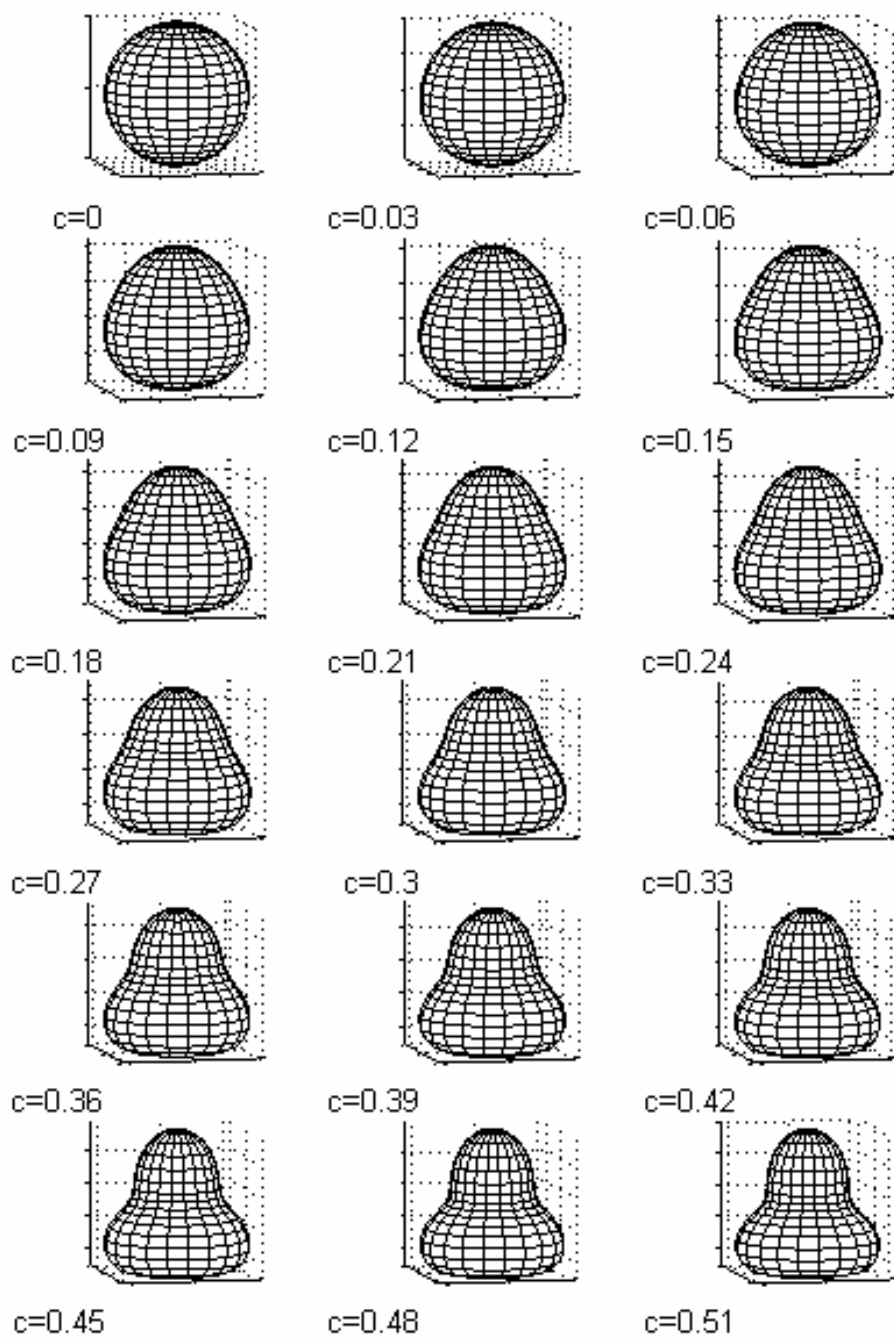


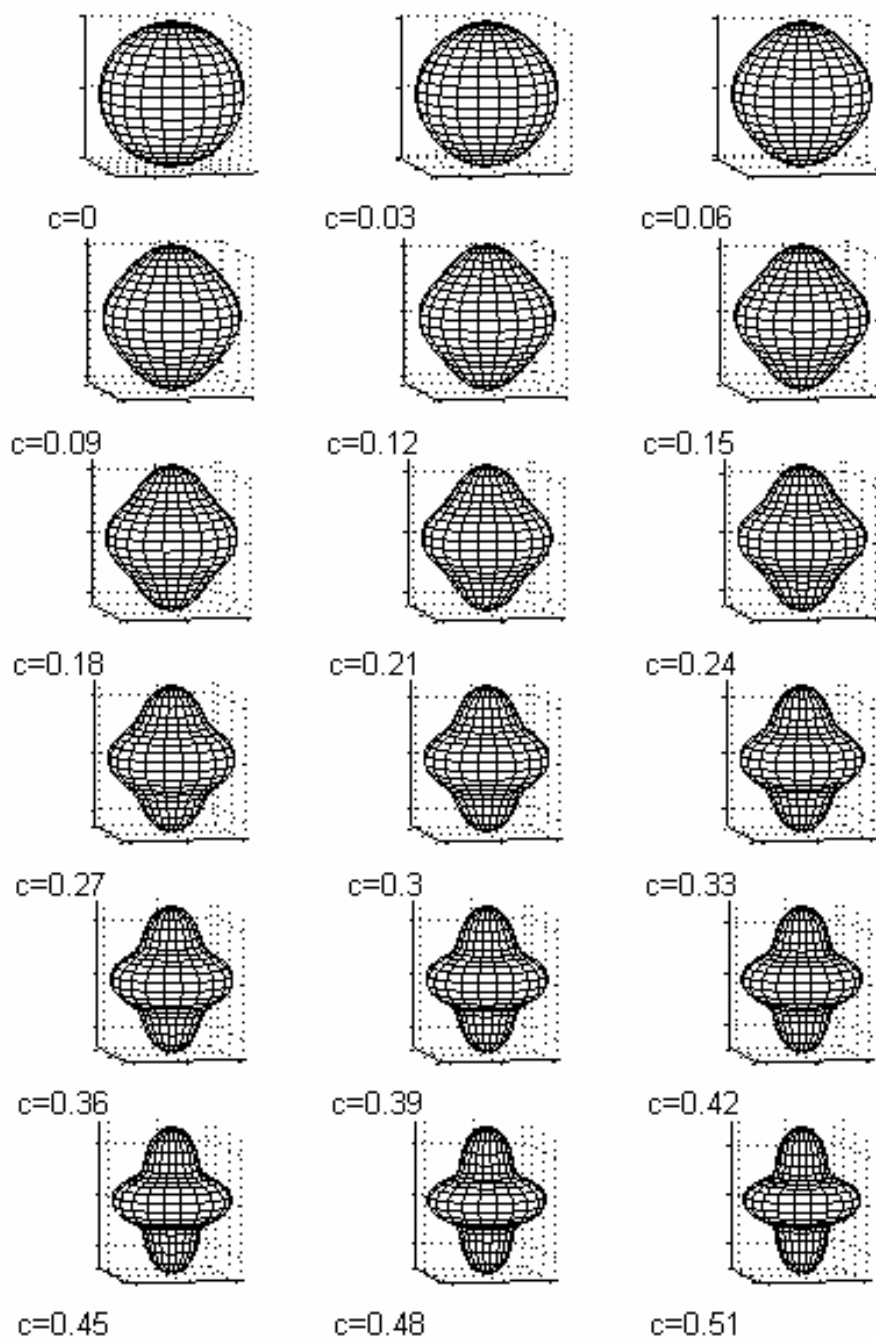
$$c=1$$



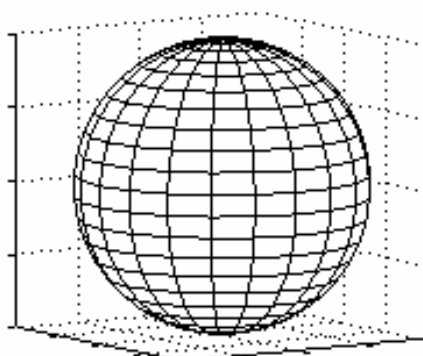
$$c=2$$

$m=0 \quad n=2$ 

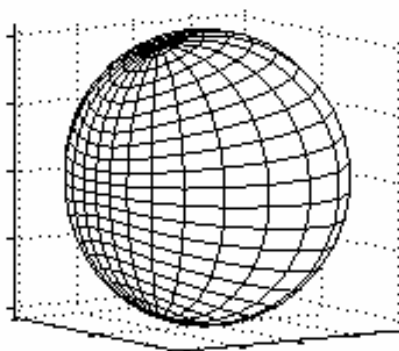
$m=0 \quad n=3$ 

$m=0 \quad n=4$ 

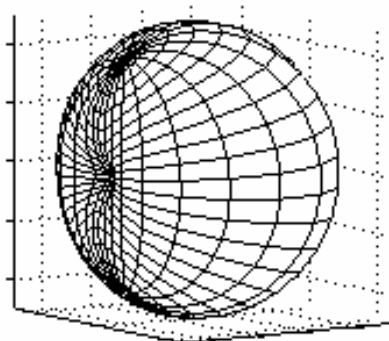
$$m=1 \quad n=1$$



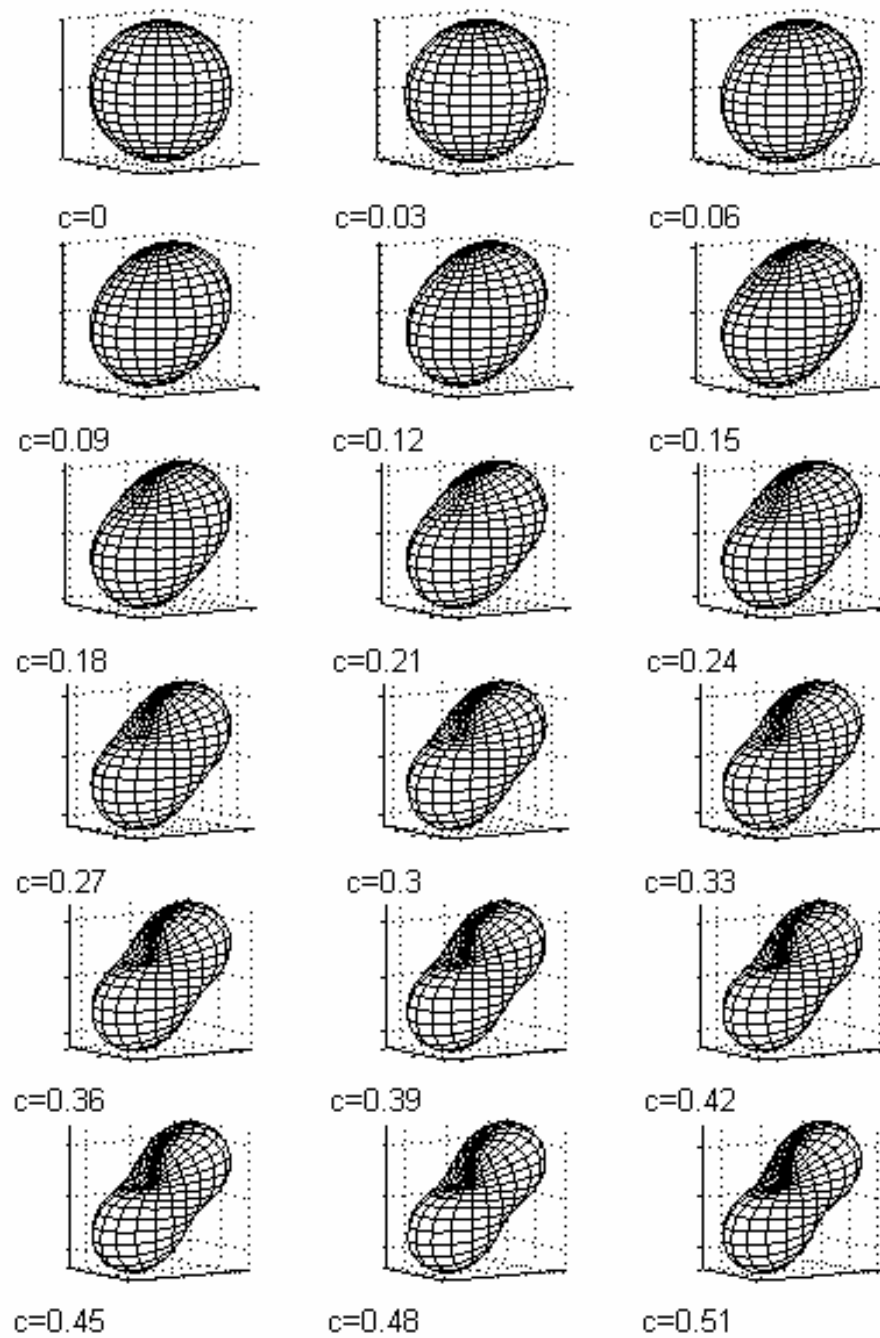
$$c=0$$

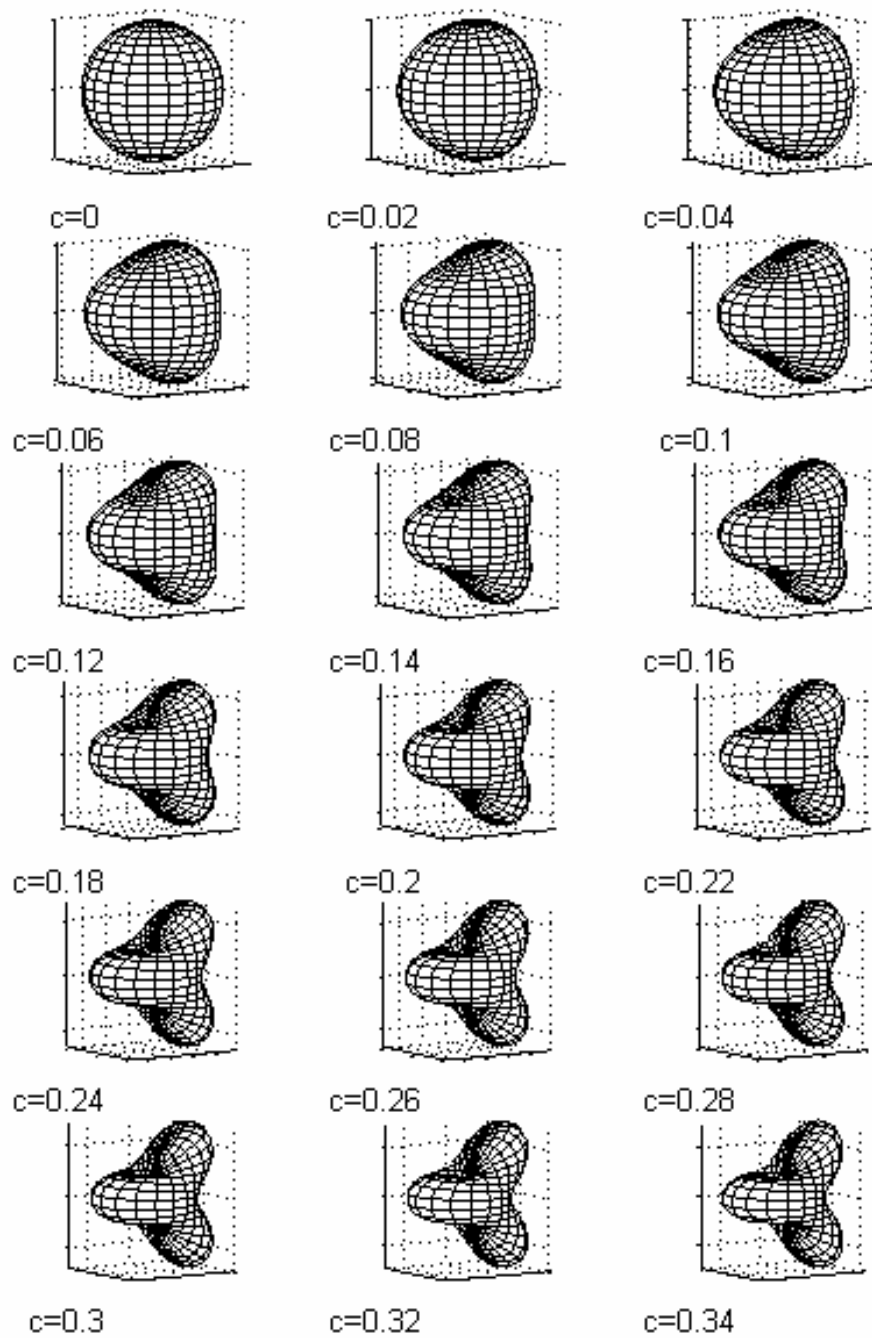


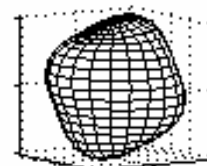
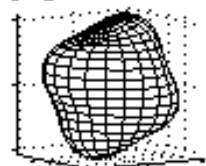
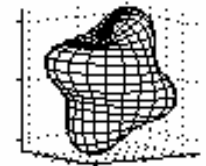
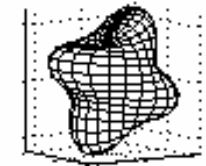
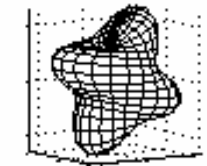
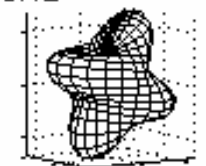
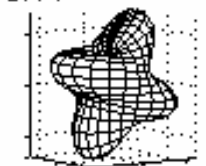
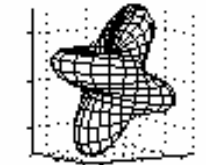
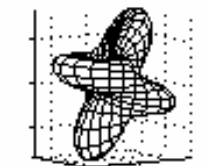
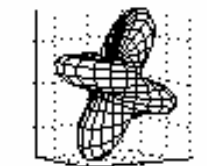
$$c=0.45$$

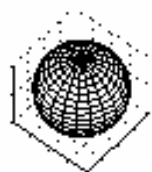
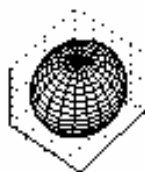
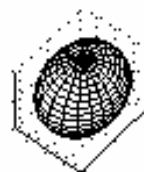
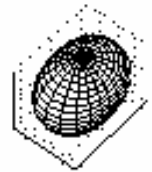
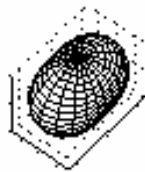
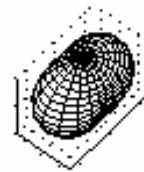
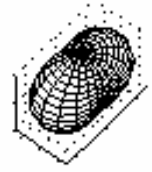
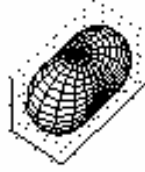
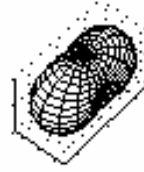
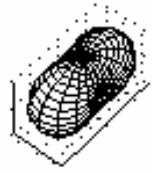
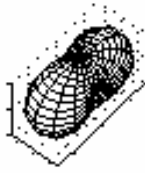
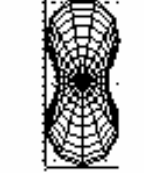
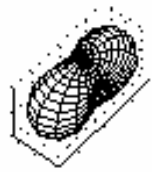
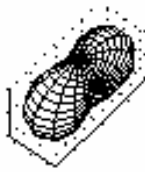
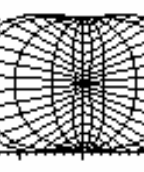
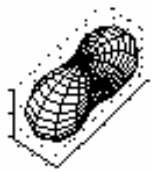
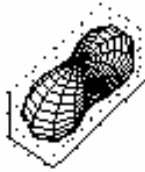


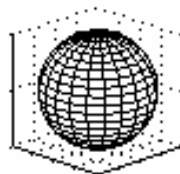
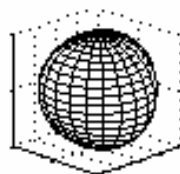
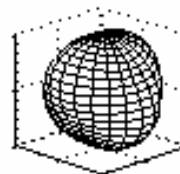
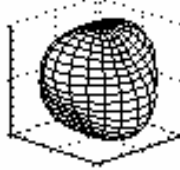
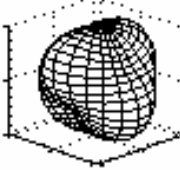
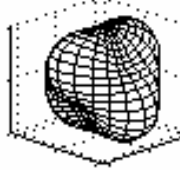
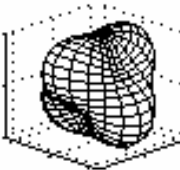
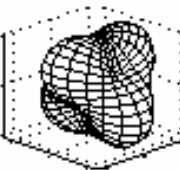
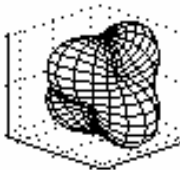
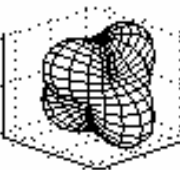
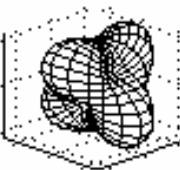
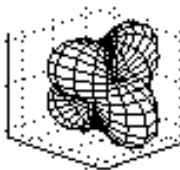
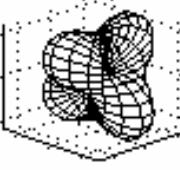
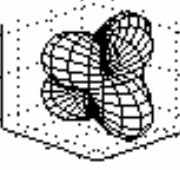
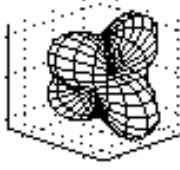
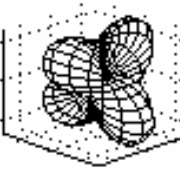
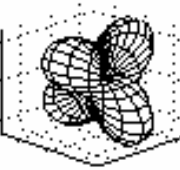
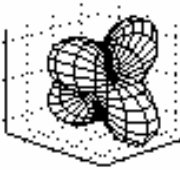
$$c=0.9$$

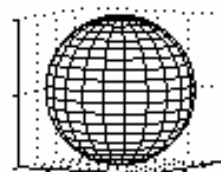
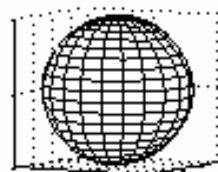
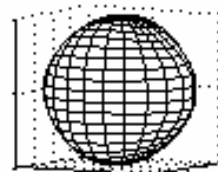
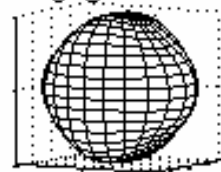
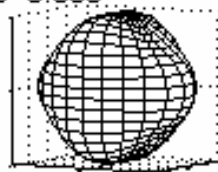
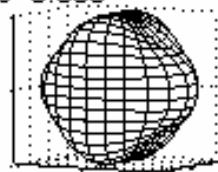
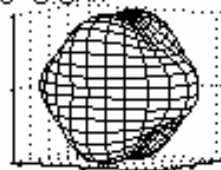
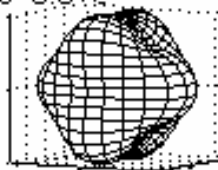
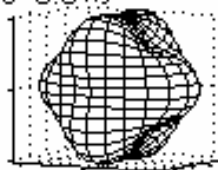
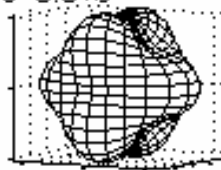
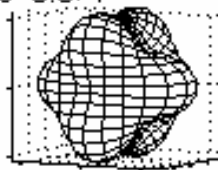
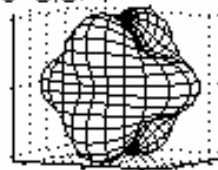
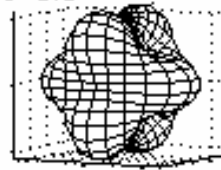
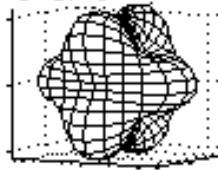
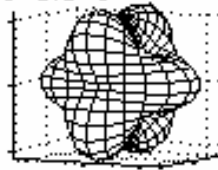
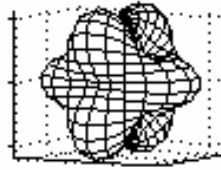
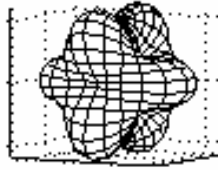
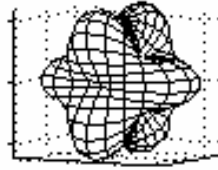
$m=1$   $n=2$ 

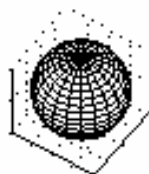
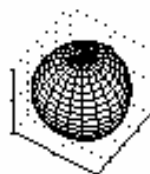
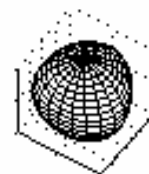
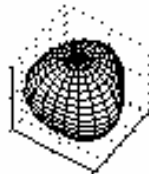
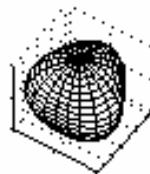
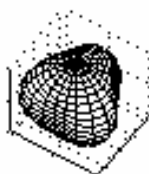
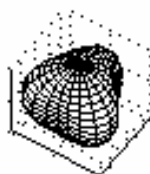
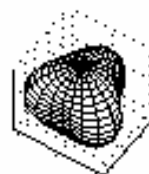
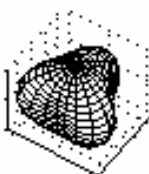
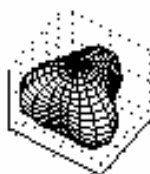
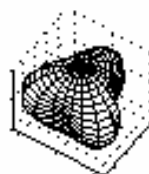
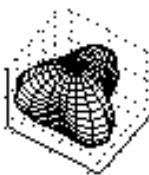
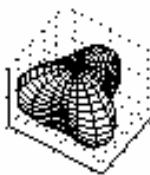
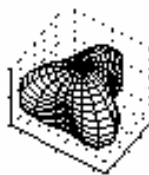
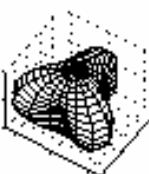
$m=1$   $n=3$ 

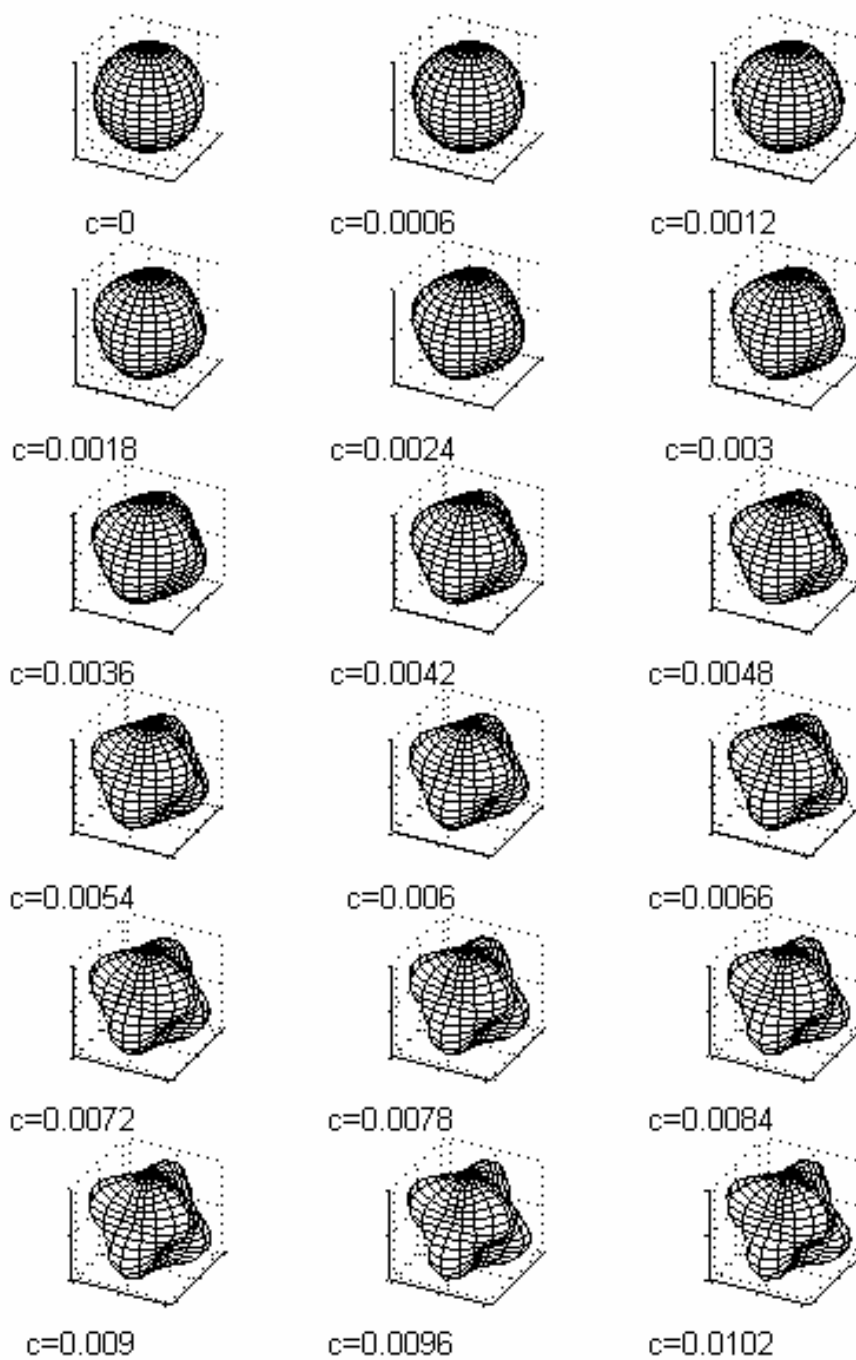
$m=1$   $n=4$  $c=0$  $c=0.02$  $c=0.04$  $c=0.06$  $c=0.08$  $c=0.1$  $c=0.12$  $c=0.14$  $c=0.16$  $c=0.18$  $c=0.2$  $c=0.22$  $c=0.24$  $c=0.26$  $c=0.28$  $c=0.3$  $c=0.32$  $c=0.34$

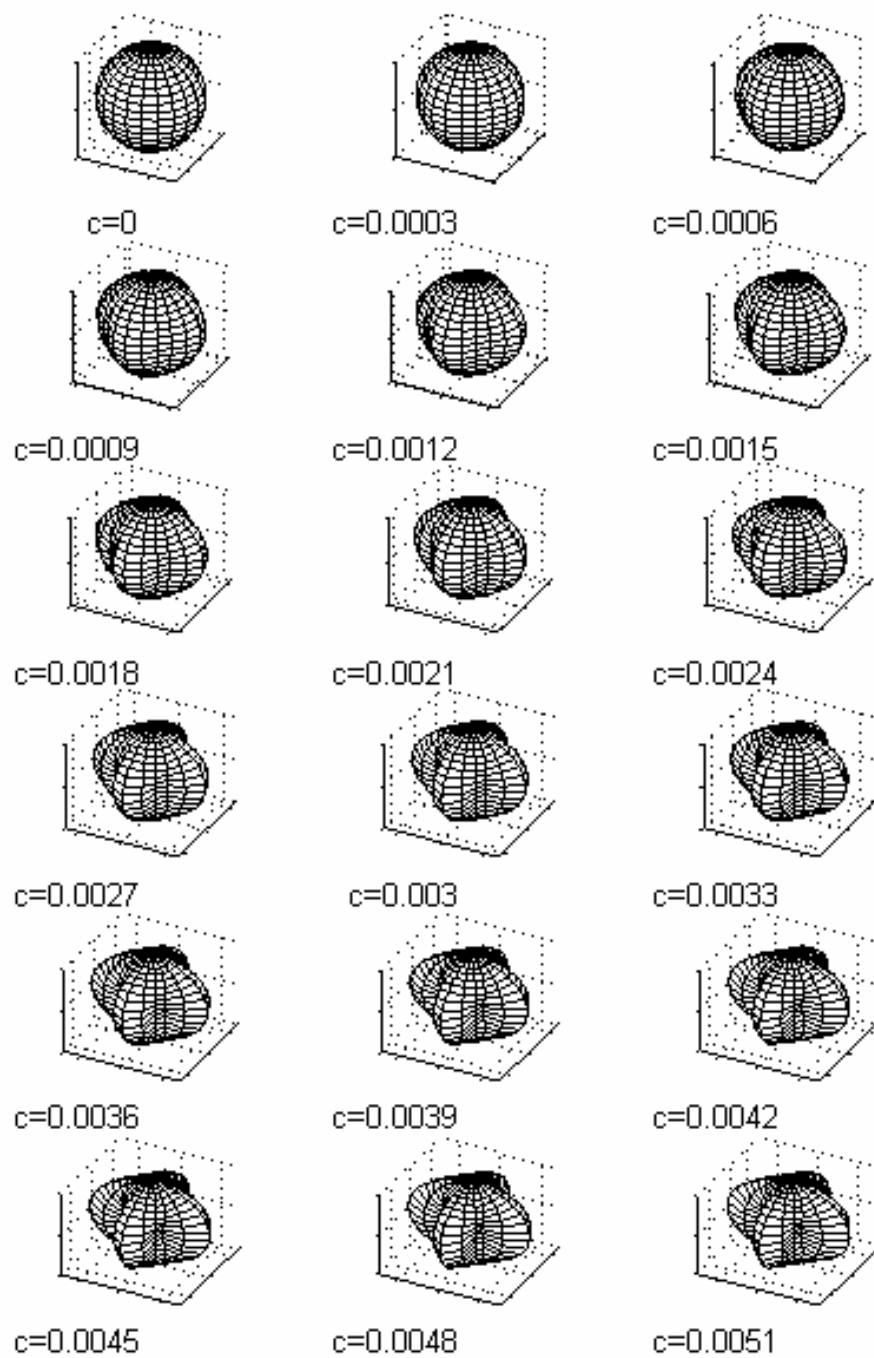
$m=2$   $n=2$  $c=0$  $c=0.02$  $c=0.04$  $c=0.06$  $c=0.08$  $c=0.1$  $c=0.12$  $c=0.14$  $c=0.16$  $c=0.18$  $c=0.2$  $c=0.22$  $c=0.24$  $c=0.26$  $c=0.28$  $c=0.3$  $c=0.32$  $c=0.34$

$m=2$   $n=3$  $c=0$  $c=0.01$  $c=0.02$  $c=0.03$  $c=0.04$  $c=0.05$  $c=0.06$  $c=0.07$  $c=0.08$  $c=0.09$  $c=0.1$  $c=0.11$  $c=0.12$  $c=0.13$  $c=0.14$  $c=0.15$  $c=0.16$  $c=0.17$

$m=2$   $n=4$  $c=0$  $c=0.003$  $c=0.006$  $c=0.009$  $c=0.012$  $c=0.015$  $c=0.018$  $c=0.021$  $c=0.024$  $c=0.027$  $c=0.03$  $c=0.033$  $c=0.036$  $c=0.039$  $c=0.042$  $c=0.045$  $c=0.048$  $c=0.051$

$m=3$   $n=3$  $c=0$  $c=0.002$  $c=0.004$  $c=0.006$  $c=0.008$  $c=0.01$  $c=0.012$  $c=0.014$  $c=0.016$  $c=0.018$  $c=0.02$  $c=0.022$  $c=0.024$  $c=0.026$  $c=0.028$  $c=0.03$  $c=0.032$  $c=0.034$

$m=3$   $n=4$ 

$m=4$   $n=4$ 

### **APPENDIX 3**

The Maple and MATLAB code used to obtain the results in this paper. The MATLAB code was used to obtain the parameters, while the Maple code was used to draw the figures with the curvature color map. The first two codes are written in MATLAB and the third code is written in MapleV version 4.

```

%This MATLAB code uses a Levenburg-Marquardt method to find the 13 parameters for the modified
%Legendre fit.
%by Cory Farley

%Originally, this code found a set of parameters using a loose tolerance(TolFun) and used them as guesses
%in a second search.
%The resulting parameters were not significantly different so the second parameter search has been cut
%out.

%First, clear the variables in memory
clear

%Then set your search parameters
options1=optimset('lsqnonlin');
options_mods1=optimset('TolX',1e-12,'MaxIter',1e10,'MaxFunEvals',1e10,'TolFun',1e-
4,'LevenbergMarquardt','on');
options1=optimset(options1,options_mods1);

%Load in the data from a txt file kept in the working directory.(The same directory in which this file is kept
%for my syntax)
data=load('data4.txt');

%In this loop, every Legendre polynomial from n=1 to 4 and m=0 to n. I couldn't find a way to designate m
%and n as integers so I was forced to do the parameter search 14 times. It calls the MATLAB file 'errfunct'
%as the model for the Lev-Mar search.
b=1;
for n1 = 1:1:4
    for m1=0:1:n1
        for n2 = 1:1:4
            for m2=0:1:n2
                m1=m1,n1=n1,m2=m2,n2=n2
                [coeff] = lsqnonlin('errfunct',[.1,1,m1,n1,.1,1,m2,n2,0,0,0,0,0],[0 0 0 0 0 0 0 0],[],options1,data);
                error=feval('errfunct',coeff,data);
                error_total(b)=sum(error);
                coeff_2(b,:)=coeff;
                b=b+1;
            end
        end
    end
end

[smallest1,index1] = min(error_total);
errtot=error_total'
mse=smallest1/length(error)
coefficients1 = coeff_2(index1,:)'

```

```

%Parameter search model (MATLAB)
%by Cory Farley

function [Err] = errfunct(C,data)

%reads in the datapoints and guess values
r=data(:,1);theta=data(:,2);phi=data(:,3);
c1=C(1);beta1=C(2);m1=round(C(3));n1=round(C(4));c2=C(5);beta2=C(6);m2=round(C(7));
n2=round(C(8));xo=C(9);yo=C(10);zo=C(11);rot1=C(12);rot2=C(13);rot3=C(14);

%sets the legendre values
leg1=legendre(n1,cos(phi));leg2=legendre(n2,cos(phi));
r_temp = beta1*(1+c1*leg1(m1+1,:)'*cos(theta*m1))+beta2*(1+c2*leg2(m2+1,:)'*cos(theta*m2));

%switches to cartesian
x_temp = r_temp .* cos(theta) .* sin(phi);
y_temp = r_temp .* sin(theta) .* sin(phi);
z_temp = r_temp .* cos(phi);

%applies an euler angle rigid body rotation
x=(x_temp*(cos(rot2)*cos(rot1)*cos(rot3)-
sin(rot2)*sin(rot3))+y_temp*(sin(rot2)*cos(rot1)*cos(rot3)+cos(rot2)*sin(rot3))-
z_temp*(sin(rot1)*cos(rot3)));
y=(x_temp*(-cos(rot2)*cos(rot1)*sin(rot3)-sin(rot2)*cos(rot3))+y_temp*(-
sin(rot2)*cos(rot1)*sin(rot3)+cos(rot2)*cos(rot3))+z_temp*(sin(rot1)*sin(rot3)));
z=(x_temp*(cos(rot2)*sin(rot1))+y_temp*(sin(rot2)*sin(rot1))+z_temp*cos(rot1));

%applies a rigid body translation and finds a value for the radius from the model
r_th = sqrt((x-xo).^2+(y-yo).^2+(z-zo).^2);

%compares the radius form the model to the radius from the data points
Err = (r-r_th).^2;

```

#This code plots the curvature maps in Maple.

```

restart;with(orthopoly):with(linalg):with(plots):
c      :=      0.0099;
beta   :=      2.1185;
m      :=      2;
n      :=      4;
alpha  :=      1.7104;
gama   :=      2.6317;
delta  :=      1.1725;
rot1   :=      0.7055;
rot2   :=      0.025;
rot3   :=      -1.7527;

legpoly[m][n]:=(-1)^m*(1-x^2)^(m/2)*diff(P(n,x),x$m);
x:=cos(phi);
r:=beta*(1+c*legpoly[m][n]*cos((theta+3*Pi/2)*m));
r_temp := subs(1-cos(phi)^2=sin(phi)^2,r);
x_temp := r_temp * cos(theta) * sin(phi);
y_temp := r_temp * sin(theta) * sin(phi);
z_temp := r_temp * cos(phi);

x:=alpha*(x_temp*(cos(rot2)*cos(rot1)*cos(rot3)-
sin(rot2)*sin(rot3))+y_temp*(sin(rot2)*cos(rot1)*cos(rot3)+cos(rot2)*sin(rot3))-
z_temp*(sin(rot1)*cos(rot3)));

y:=gama*(x_temp*(-cos(rot2)*cos(rot1)*sin(rot3)-sin(rot2)*cos(rot3))+y_temp*(-
sin(rot2)*cos(rot1)*sin(rot3)+cos(rot2)*cos(rot3))+z_temp*(sin(rot1)*sin(rot3)));

z:=delta*(x_temp*(cos(rot2)*sin(rot1))+y_temp*(sin(rot2)*sin(rot1))+z_temp*cos(rot1));
PP:=[x,y,z];
plot3d(PP,theta=0..2*Pi, phi=0..Pi, scaling=constrained, style=patch);
PP1:=diff(PP,theta);
PP2:=diff(PP,phi);
PP11:=diff(PP1,theta);
PP22:=diff(PP2,phi);
PP12:=diff(PP1,phi);
E:=dotprod(PP1,PP1);
F:=dotprod(PP1,PP2);
GG:=dotprod(PP2,PP2);
n:=normalize(crossprod(PP1,PP2));
LL:=dotprod(PP11,n);
M:=simplify(dotprod(PP12,n));
N:=dotprod(PP22,n);

lambda1:=1/2/(-N*F+M*GG)*(-LL*GG+N*E+(LL^2*GG^2-2*LL*GG*N*E+N^2*E^2-
4*N*F*M*E+4*N*F^2*LL+4*M^2*GG*E-4*M*GG*LL*F)^(1/2));

lambda2:=1/2/(-N*F+M*GG)*(-LL*GG+N*E-(LL^2*GG^2-2*LL*GG*N*E+N^2*E^2-
4*N*F*M*E+4*N*F^2*LL+4*M^2*GG*E-4*M*GG*LL*F)^(1/2));

kappa1:=(LL+2*M*lambda1+N*(lambda1)^2)/(E+2*F*lambda1+GG*(lambda1)^2);

```

```
kappa2:=(LL+2*M*lambda2+N*(lambda2)^2)/(E+2*F*lambda2+GG*(lambda2)^2);  
plot3d(kappa1,theta=0..2*Pi,phi=0..3,color=kappa1+1);  
plot3d(PP,theta=0..2*Pi,phi=0..3,color=kappa1+1);  
plot3d(kappa2,theta=0..2*Pi,phi=0..3,color=kappa2+1);  
plot3d(PP,theta=0..2*Pi,phi=0..3,color=kappa2+1);
```

**VITA**

Name: Cory Farley

Education: B.S. Mechanical Engineering, Texas A&M University  
M.S. Biomedical Engineering, Texas A&M University

Permanent Address: 4600 Buffalo Trl  
Amarillo, TX 79109